JBC Papers in Press. Published on January 15, 2015 as Manuscript M114.610899
The latest version is at http://www.jbc.org/cgi/doi/10.1074/jbc.M114.610899

Silver nanoparticles induce degradation of the endoplasmic reticulum stress sensor Activating Transcription Factor-6 leading to activation of the NLRP-3 inflammasome

Jean-Christophe Simard[1*], Francis Vallieres[1], Rafael de Liz[1], Valerie Lavastre[1] and Denis Girard[1]

[1] Laboratoire de recherche en inflammation et physiologie des granulocytes, Université du Québec, Institut National de la Recherche Scientifique-Institut Armand-Frappier. Laval, Québec, Canada.

Running Title: Silver nanoparticles in ER stress and activation of the inflammasome

[*]Corresponding authors: Jean-Christophe Simard and Denis Girard, Institut National de la Recherche Scientifique-Institut Armand-Frappier, 531 Boulevard des Prairies, Laval, Québec, Canada, H7V1B7. E-mail: J-Christophe.Simard@iaf.inrs.ca; Denis.girard@iaf.inrs.ca

Keywords: Silver nanoparticles; Endoplasmic reticulum stress; NLRP-3 inflammasome; pyroptosis; caspase-4.

Background: Some nanoparticles are known to induce endoplasmic reticulum (ER) stress and lead to cell death.
Results: Silver nanoparticles induce ATF-6 degradation, leading to activation of the NLRP-3 inflammasome and pyroptosis.
Conclusion: ATF-6 is an important target to silver nanoparticles.
Significance: Our results provide a new link between ER stress and activation of the NLRP-3 inflammasome.

ABSTRACT

In the past decade, the increasing amount of nanoparticles (NPs) and nanomaterials used in multiple applications led the scientific community to investigate the potential toxicity of NPs. Many studies highlighted the cytotoxic effects of various NPs, including titanium dioxide, zinc oxide and silver nanoparticles (AgNPs). In a few studies, endoplasmic reticulum (ER) stress was found to be associated with NP cytotoxicity leading to apoptosis in different cell types. In this study, we report for the first time that silver nanoparticles of 15 nm ($AgNP_{15}$), depending on the concentration, induced different signature ER stress markers in human THP-1 monocytes leading to a rapid ER stress response with degradation of the ATF-6 sensor. Also, $AgNP_{15}$ induced pyroptosis and activation of the NLRP-3 inflammasome as demonstrated by the processing and increased activity of caspase-1, secretion of IL-1β and ASC pyroptosome formation. Transfection of THP-1 cells with siRNA targeting NLRP-3 decreased the $AgNP_{15}$-induced IL-1β production. Absence of caspase-4 expression resulted in a significant reduction of pro-IL-1β. However, caspase-1 activity was significantly higher in caspase-4 deficient cells compared to WT cells. Inhibition of $AgNP_{15}$-induced ATF-6 degradation with Site-2 protease inhibitors completely blocked the effect of $AgNP_{15}$ on pyroptosis and secretion of IL-1β, indicating that ATF-6 is crucial for the induction of this type of cell death. We conclude that $AgNP_{15}$ induce degradation of the ER stress sensor ATF-6, leading to activation of the NLRP-3 inflammasome regulated by caspase-4 in human monocytes.

INTRODUCTION

Nanoparticles (NPs) are used in many applications and in a variety of sectors, including textile, aerospatial, electronics and medical healthcare. Silver nanoparticles (AgNPs) are among the most commonly used NPs in nanomedicine, mainly because of their potent antimicrobial properties, increasing the interest to use them for drug

delivery (1). Indeed, silver ions and nanosilver were shown to be highly toxic for various types of microorganisms, including *Pseudomonas* spp. and *Escherichia* spp (2,3). Even if potential exposure of humans to AgNPs is already high, it will certainly increase in the becoming years. Since the toxicity of AgNPs in humans is not fully understood, it is highly relevant to investigate their mode of action at the cellular and molecular level in humans.

Endoplasmic reticulum (ER) stress leads to unfold protein response (UPR), a major hallmark of cytotoxicity. To date, three ER-stress sensors have been documented: Protein kinase RNA-like Endoplasmic Reticulum Kinase (PERK), Inositol-Requiring enzyme 1 (IRE-1) and Activating Transcription Factor 6 (ATF-6). IRE-1 and PERK both contain cytoplasmic kinase domains known to be activated by homodimerisation and autophosphorylation in the presence of ER stressors (4-6). In the case of ATF-6, accumulation of unfolded proteins induce ATF-6 transition to the Golgi, where it is cleaved by two transmembrane proteins, Site-1 and Site-2 proteases (7). ATF-6 cleavage yields a cytoplasmic protein acting as an active transcription factor. While short-termed ER-stress events leads to pro-survival transcriptional activities, prolonged ER stress activates the major apoptotic pathways (8,9). Moreover, ER-stress related events were recently proposed as an early biomarker for nanotoxicological evaluation (10). A few studies have reported ER-stress related events induced by NPs in human cell lines and in zebrafish (10-12).

Pyroptosis, a type of programmed cell death sharing common features with apoptosis and necrosis leads to the assembly of the inflammasomes and the formation of large structures called pyroptosomes characterized by aggregation of Apoptosis-associated Speck-like protein containing a Card domain (ASC) (13). Formation of pyroptosomes allows recruitment and processing of caspase-1 into two active fragments, p10 and p20 (14). Caspase-1 controls processing and secretion of IL-1β, one of the most potent endogenous pyrogenic molecules. IL-1β is responsible for inflammatory cell infiltration and is known to induce cyclooxygenase, increase expression of adhesion molecules, production of reactive oxygen species (ROS) and other inflammatory soluble mediators (15). Secretion of high concentrations of IL-1β is also associated with chronic inflammatory conditions, including rheumatoid arthritis and inflammatory bowel diseases (16). Interestingly, treatment of some auto-immune diseases with anti-IL-1β antibodies results in significant reduction of disease severity and symptoms. Pyroptosis also leads to the release of cytosolic content via formation of pore in the cellular membrane, thereby increasing the inflammatory process (17). Some NPs were shown to induce pyroptosis in human cells, namely carbon nanotubes, carbon black NPs and AgNPs (18-20). Therefore, studying the impact of several distinct NPs in the regulation of the inflammasome has become highly relevant for investigating their toxicity.

In this study, we show that low concentrations of silver nanoparticles of 15 nm ($AgNP_{15}$) induces ER-stress response but did not led to cell death, whereas higher concentrations resulted in atypical ER-stress response associated with ATF-6 degradation and pyroptosis cell death through NLRP-3 inflammasome activation. Our data suggest a link between these two processes.

EXPERIMENTAL PROCEDURES

Reagents- $AgNP_{15}$ were obtained from US nanoresearch (Houston, TX). Staurosporine and Adenosine-5-Triphosphate (ATP) were purchased from Sigma-Aldrich (St. Louis, MO). Caspase-1, Caspase-3, Caspase-7 and Phospho-eIF2α antibodies were purchased from Cell Signaling (Danvers, MA). GAPDH (FL), ASC, caspase-4, Phospho-PERK, ATF-6α (full length), GRP-78 and pro-IL-1β (H-153) specific antibodies were obtained from Santa Cruz Biotechnology (Santa Cruz, CA). NLRP-3/NALP-3 antibody was purchased from Enzo Life Sciences (Farmingdale, NY). RPMI-1640, HEPES, penicillin and streptomycin (Pen/Strep), heat-inactivated fetal bovine serum (FBS), opti-MEM medium and Hank's balanced salt solution (HBSS) were purchased from Life technologies (Camarillo, CA). All secondary antibodies were purchased

from Jackson Immuno-Research Laboratories (West Grove, PA). Ultrapure LPS from *Salmonella spp.* was purchased from Invivogen (San Diego, CA). Phospho-IRE-1, total IRE-1 and ATF-6 (cleaved form) were purchased from Pierce (Rockford, IL). HSP-70 and HSP-90 antibodies were purchased from Stressgen Biotechnologies (San Diego, CA) Anti-Sterol Regulatory Element Binding Protein-1 (SREBP-1) was purchased from EMD Millipore (Temecula, CA).

Characterization of $AgNP_{15}$ - The $AgNP_{15}$ suspension obtained from the manufacturer was examined by transmission electronic microscopy using a Hitachi H-7100 transmission electron microscope (21). The size distribution and electric charge (zeta potential) of $AgNP_{15}$ were determined by Dynamic Light Scattering (DLS) using a Malvern Zetasizer Nano-ZS (model ZEN3600; Malvern Instruments Inc., Westborough, MA, USA). Measurements were performed at 1, 5, 10 and 25 µg/ml $AgNP_{15}$ in RPMI-1640 with HEPES and 100 U/ml penicillin, 100 µg/ml streptomycin (further referred to as RPMI) + 10% heat-inactivated FBS, at 37°C.

Cell culture - Wild type human monocytic THP-1 (WT) were purchased from ATCC. Stable caspase-4 deficient (clone TB) THP-1 cells and the corresponding cell line containing a scrambled sequence (VC) were kindly given by Dr. Alan G. Porter (22). These cells line were cultured in RPMI. Cell density never exceeded 1 X 10^6 cells/mL and viability was evaluated before each experiment and was always above 95 %. For primary culture of monocytes and macrophages, PBMCs were first isolated from healthy blood donors after centrifugation over ficoll-Hypaque gradient, as previously published (23). For monocyte isolation, 25x10^6 PBMC were incubated at 37˚C in a 5% CO_2 atmosphere for 2h in RPMI containing 10% autologous heat-inactivated serum in a Petri dish. Monocytes obtained by removing the non-adherent PMBC were further incubated in RPMI–10% heat-inactivated FBS for another 12h. The monocytes were washed twice with HBSS without Ca^{2+} and Mg^{2+} with 2 mM EDTA and harvested with a cell scraper. Human monocyte–derived macrophages (HMDM) were generated by incubating 2 X 10^6 PBMCs at 37˚C in a 5% CO_2 atmosphere for 2h in RPMI with 10% heat-inactivated autologous serum in 48-well plates. Cells were then washed twice with warm HBSS and further incubated in RPMI 1640 supplemented with 2 ng/ml GM-CSF for seven days, with medium renewal every three days, to obtain macrophages.

Transfection of siRNA - THP-1 cells were transfected with Silencer Select Pre-designed siRNA from Ambion (Austin, TX) according to the manufacturer's protocol. Briefly, 5 X 10^5 cells were suspended in 1 mL of opti-MEM reduced serum medium containing 2 µL of Lipofectamine RNAiMAX Reagent (Life Technologies) and 10 µM of siRNA targeting: NLRP-3 (sense GGAGAGACCUUUAUGAGAATT; antisense UUCUCAUAAGGUCUCUCCTG) or control non-silencing siRNA (sense UUCUCCGAACGUGUCACGUTT, antisense ACGUGACACGUUCGGAGGAGAATT). After 24-48h, cells were washed and treated with the indicated agents.

Cell death assessment - For assessment of cell death, THP-1 cells were treated for 1h or 24h with the indicated agents. After different periods of time, cells were harvested and washed twice in PBS and then stained with FITC-Annexin-V and propidium iodine, according to the manufacturer's protocol (Life technologies). Cells were analyzed by flow cytometry using a BD FASCscan.

Western blot analysis - Cells were stimulated at 1 X 10^6 cells/mL with the indicated agonists for various periods of time, as specified. At the end of the incubation periods, cells were lysed in Laemmli's sample buffer (0.25 M Tris-HCl [pH 6.8], 8% SDS, 40% glycerol, and 20% 2-ME), and aliquots corresponding to 5 x 10^5 cells were loaded onto 10% SDS-PAGE and transferred to nitrocellulose membranes for the detection of specific proteins. Membranes were blocked for 1h at room temperature in 5% non-fat dry milk. After washing, the primary antibodies were added at a final dilution of (1:1000) in TBS-Tween 0.15%. The membranes were kept overnight at 4°C, then washed with TBS-Tween and incubated for 1h at

room temperature with the appropriate secondary HRP antibody 1:25,000 in TBS-Tween followed by several washes. Protein expression was revealed using Luminata Forte Western HRP Substrate (Millipore). Membranes were stripped with ReBlot Plus Strong (Millipore) and reprobed to confirm equal loading of proteins. Chemiluminescence was revealed with a chemiDocTM MP Imaging system from Bio-Rad.

Assembly of pyroptosome by confocal microscopy- THP-1 cells were incubated on poly-L-lysine coverslips for 30 min at 37 °C and then incubated with the indicated agonist for 30 min. In some experiments, cells were primed with LPS (100 ng/mL) for 4h. Coverslips were then washed three times with PBS and fixed in 3.7% parafolmaldehyde. After three washes in PBS, cells were permeabilized in PBS containing 0.1% saponin and 0.05% Tween-20. Cells were blocked with a blocking solution containing 5% goat serum, 1% BSA and 1% dry fat milk and stained with mouse anti-ASC (2 µg/mL) primary antibody. After three washes with PBS, cells were incubated with Alexa-Fluor®-488 goat anti-mouse IgG (1:500) secondary antibody. Cells were washed three times with PBS and coverslips were mounted using ProLong Gold® antifade reagent containing DAPI. Cells were then visualized with a Zeiss LSM780 on Axio Observer Z1confocal microscope using a Plan-Apochromat 63x 1.4NA Oil DIC objective. Five fields with at least 50 cells/field were evaluated for the presence of pyroptosome.

Caspase-1 assay - Caspase-1 activity was measured with Caspase-1 Colorimetric Assay kit (R&D Systems) as previously described (24). Briefly, 4 x 10^6 cells were stimulated with agonists for the indicated periods of time and lysed with ice-cold lysis buffer after incubation for 10 min on ice. Cells were centrifuged at 10,000 x g for 1 min and supernatants were used for enzymatic reaction. Caspase-1 colorimetric susbtrate (WEHD-pNA) was added to each reaction mixtures with the corresponding volume of cell lysate, reaction buffer and DTT. The plate was incubated for 2h at 37 °C. After incubation, lectures were read with a microplate reader using a wavelength of 405 nm. Results are expressed as fold increase of caspase-1 activity.

Caspase-3 and -4 activity assays. Caspase-3 and caspase-4 activity assays were performed as previously published with few modifications (25). Briefly, THP-1 cells (1 X 10^6 cells/mL) were stimulated as indicated in figure legends. Cells were washed twice in PBS and disrupted using a lysis buffer containing Hepes 25 mM pH 7.5, EDTA 5 mM, 5 mM $MgCl_2$, DTT 10 mM, Triton X-100 0.5% and protease inhibitor cocktail (Pierce, Thermo Fisher). Protein concentration was determined using the Bradford assay. An amount of 10 µg of proteins was mixed in 200 µL of reaction buffer containing Hepes 50 mM, sucrose 10%, CHAPS 0.1%, DTT 10 mM with 100 µM of the caspase-3 (DEVD-pNA) or caspase-4 (LEVD-pNA) substrate for 2h at 37 °C. Cleavage of the caspase substrate was monitored using a spectrophotometer at 405 nm.

Transmission Electronic Microscopy - Cells were treated with 25 µg/ml $AgNP_{15}$ or buffer for 1h and then fixed with glutaraldehyde (2.5%) and examined by transmission electron microscopy, as above.

IL-1β production - The measurement of IL-1β was determined with a commercially available ELISA kit (Life technologies). THP-1, primary monocytes or macrophages were incubated with the indicated agonists for 1h in a 24-wells plate in RPMI- 10% FBS or autologous serum. In some experiments, cells were pre-incubated with LPS (100 ng/mL) for 4h. Supernatants were harvested after centrifugation and stored at -80°C before determining the concentration of IL-1β.

Statistical Analysis - Experimental data are expressed as means ± SEM. One-way ANOVA (Dunnett multiple-comparison test) and two-way ANOVA (Bonferroni post-test) were performed using Graph-Pad Prism (version 5.01). Differences were considered statistically significant as followed: * $p \leq 0.05$, ** $p \leq 0.01$, and *** $p \leq 0.005$ vs control or appropriate diluent.

RESULTS

Characterization of $AgNP_{15}$ - We first characterized $AgNP_{15}$ from the manufacturer stock solution by TEM confirming a diameter close to

15 nm, but indicating also that the suspension contains NPs with different smaller and greater diameters (**Fig. 1A**). Since RPMI-1640 supplemented with 10% FBS was the medium used for all experiments throughout this study, the size distribution and zeta potential of $AgNP_{15}$ were determined by DLS for all tested concentrations in this medium at 37°C, the temperature at which cells were incubated. As shown in **Fig. 1B** and **Table 1**, the DLS analysis revealed a tri-modal size distribution for a concentration of 1, 5, and 25 µg/mL and bi-modal at 10 µg/mL with a polydispersion index of 0.4 ± 0.3, 0.4 ± 0.3, 0.2 ± 0.1 and 0.3 ± 0.1 (n=6) for 1, 5, 10 and 25 µg/mL, respectively. The zeta potential was stable ranging from -8.4 ± 0.4 to -9.5 ± 1.0 mV.

$AgNP_{15}$ induce morphological changes in human THP-1 monocyte cells - **Fig.2** illustrates that, after 24h of treatment, the cell morphology remained unchanged at a concentration of 1 or 5 µg/mL $AgNP_{15}$. However, morphological changes became apparent at 10 µg/mL of $AgNP_{15}$ where numerous vacuoles were observed in the cytosol (e). Cell morphology was markedly altered at 25 µg/mL $AgNP_{15}$ (f) an effect that is clearly different from that of the apoptosis-inducing agent staurosporine, suggesting a different type of cell death.

$AgNP_{15}$ are internalized in THP-1 cells - We next investigated potential internalization of $AgNP_{15}$, since we previously reported that silver nanoparticles of 20 nm ($AgNP_{20}$) could be found inside human neutrophils, another cell type of myeloid origin (26). As illustrated in **Fig. 3**, incubation of $AgNP_{15}$ with THP-1 cells lead to internalization of nanoparticles in the cytosol and nucleus as determined by TEM (**Fig. 3**). Larger aggregates of $AgNP_{15}$ were visibly uptaken by a mechanism requiring the formation of phagosomes/vacuoles while well dispersed or small aggregates were mainly found inside the nucleus. Well dispersed nanoparticles were also found in the cytosol but were not internalized inside vacuoles.

$AgNP_{15}$ induce ER-stress related event - A 24h treatment of cells with $AgNP_{15}$ resulted in a dose-dependent dephosphorylation of IRE-1, suggesting that this pathway was not activated (**Fig. 4A)**. While the PERK-pathway was strongly activated with 1-10 µg/mL of $AgNP_{15}$, it remains similar to basal level with a treatment with 25 µg/mL. In addition, low concentrations of $AgNP_{15}$ induced synthesis of HSP-70 while the higher concentration induced degradation of HSP-90. GRP-78 expression levels remained unchanged in all tested conditions but thapsigargin (Tg), the positive control. While the expression level of ATF-6 remained similar in cells treated with 0-10 µg/mL $AgNP_{15}$, this protein was degraded at 25 µg/mL, despite the fact that an equivalent of proteins was loaded (see GAPDH). Interestingly, degradation of ATF-6 occurred rapidly after 1h (**Fig. 4B**). Degradation of other components such as HSP-70 was also observed while the expression level of total IRE-1 and HSP-90 remained relatively stable after 1h of stimulation. These results suggest that $AgNP_{15}$ induce ER stress related events in human THP-1 cells.

$AgNP_{15}$ induce a rapid cell death distinct than apoptosis - As prolonged ER-stress response is usually associated with apoptosis, we next investigated the role of *$AgNP_{15}$* in THP-1 cell death. After only 1h, cells treated with 25 µg/ml $AgNP_{15}$ were annexin-V and PI positive, whereas cells treated with the proapoptotic agent staurosporine were negative for both markers (**Fig. 5A** and **Fig. 5B**). However, after 24h, cells were annexin-V and PI positive whether they were treated with $AgNP_{15}$ or staurosporine. This suggests that $AgNP_{15}$, at 25 µg/ml, induce a cell death that is different than staurosporine-induced apoptosis. To confirm this hypothesis, we next monitored the processing of several important caspases, including the executioner caspase-3 and caspase-7, and the inflammatory caspase-4, known to be associated with ER stress-induced apoptosis (27). As illustrated in **Fig. 5C**, Staurosporine induced processing of caspase-3, caspase-4 and caspase-7, but not $AgNP_{15}$ at 1, 5, or 10 µg/ml. At 25 µg/ml, $AgNP_{15}$ was found to induce the processing of caspase-4 and caspase-7 but not caspase-3. We also observed a variation in the expression of level of GAPDH in staurosporine treated cells, a phenomenon previously observed at the mRNA level in neutrophils (28). However, membrane coloration revealed equivalent amount of proteins (*data not shown*). The activity of

caspase-3 and caspase-4 was also monitored using a caspase assay. Only the positive control staurosporine induced activation of caspase-3, while $AgNP_{15}$ strongly activated caspase-4 at 25 µg/mL (**Fig. 5D-E)**. These results indicate that AgNPs-induced cell death is distinct from apoptosis.

$AgNP_{15}$ induce pyroptosis and activation of the inflammasome - Knowing that activation of caspase-4 and -7 are associated with activation of the inflammasome (13,29,30), in addition to the loss of membrane integrity observed after PI-staining (this report), we next investigated the role of $AgNP_{15}$ in the activation of inflammasomes. Since pyroptosis, another type of cell death, is dependent on caspase-1, we also followed its processing as well as its activation and other components of the NLRP-3 inflammasome. $AgNP_{15}$ treatment at 25 µg/ml resulted in the presence of the p20 caspase-1 fragment. (**Fig. 6A**). Such caspase-1 processing was also observed at 25 µg/ml $AgNP_{15}$ when cells were pre-treated with LPS, suggesting that the effect is due to AgNP alone independently of the LPS pre-treatment. Of note, in absence of LPS, pro-IL-1β was undetectable, but when cells were pretreated with LPS, a strong expression of pro-IL-1β was observed. ASC expression remained relatively constant whether or not cells were pre-treated with LPS. Because $AgNP_{15}$ induced processing of caspase-1, suggesting that it induces its activity, we next verified if $AgNP_{15}$ could activate caspase-1, using a specific activity assay. As shown in **Fig. 6B**, the caspase-1 assay revealed that 25 µg/ml $AgNP_{15}$ significantly increased caspase-1 activity. Also, the activity of caspase-1 was found to correlate with the secretion of IL-1β in the extracellular milieu where 25 µg/ml $AgNP_{15}$ significantly increased the IL-β secretion from 9.5 ± 2.8 pg/ml to 298.2 ± 52.7 pg/ml (**Fig. 6C**). Of note, secretion of mature IL-1β required priming with LPS since unstimulated cells failed to secrete this cytokine (**Fig. 11B**). We have next investigated the importance of $AgNP_{15}$ internalization for its effect on IL-1β secretion. Therefore, cells were pre-treated or not with the endocytosis dynamin inhibitor (dynasore) or with the actin depolarizing agent (cytochalsin D) before incubation with $AgNP_{15}$. Cytochalsin D reduced slightly the secretion of IL-1β induced by $AgNP_{15}$ while dynasore has no effect on its secretion (**Fig. 6D**). These results suggested that internalization of $AgNP_{15}$ might be dispensable for their effect on secretion of IL-1β.

Formation of pyroptosome is a well-documented feature of pyroptosis cell death, characterized by aggregation of ASC proteins into normally one aggregate as observed in murine macrophages or in human monocyte THP-1 cells (13,14). Therefore, we have followed the formation of this structure by confocal microscopy using an ASC-specific antibody. As illustrated in **Fig. 7A**, $AgNP_{15}$ induced formation of a pyroptosome structure (arrow) similar to that of ATP (positive control) (31), whereas the localization of ASC protein remained diffuse in control cells. The number of cells expressing pyroptosome structures was also quantified in response to 25 µg/ml $AgNP_{15}$ where close to 20% of cells showed the presence of ASC pyroptosome in the experimental conditions tested (**Fig.7B**).

$AgNP_{15}$ induce activation of the NRLP-3 inflammasome - Several inflammasomes are found in monocytes including NLRP-3, the most common and best characterized inflammasome (32). To determine whether $AgNP_{15}$ induce specific activation of the NLRP-3 inflammasome, siRNA targeting NLRP-3 were transfected in THP-1 cells. NLRP-3 expression levels were then followed by western blot to determine the efficiency of transfection. A marked decreased of NLRP-3 protein expression was observed after a transfection period of 48h, but not 24h (**Fig. 8A** and **Fig. 8B**). Therefore, we next selected this 48h time point for further experiments. As illustrated in **Figure 8C**, a significant decrease in IL-1β secretion was observed in cells transfected with silencing NLRP-3 siRNA, confirming that $AgNP_{15}$ activate the NLRP-3 inflammasome. Activation of the NLRP-3 inflammasome is dependent on caspase-1 (33). We have therefore evaluated the importance of caspase-1 in the activation of the NLRP-3 inflammasome by $AgNP_{15}$. Caspase-1 was found to be crucial for activation of this inflammasome since its inhibition with YVAD-CHO completely abolished the secretion of IL-1β, thereby confirming the importance of caspase-1 in this process (**Fig. 8D)**.

Caspase-4 regulates the activation of the NRLP-3 inflammasome - Caspase-4 is known to be required for the activation of the inflammasome through interaction with caspase-1 (30). Since $AgNP_{15}$ induced activation of the NLRP-3 inflammasome and also processing of caspase-4, we tested whether caspase-4 was involved in this process. To do so, we used caspase-4 deficient THP-1 cells (22,34) to characterize the role of this caspase in $AgNP_{15}$-induced pyroptosis. Absence of caspase-4 protein expression was confirmed in the caspase-4 deficient THP-1 cell clone TB in contrast to the clone VC (vector control) where caspase-4 was strongly expressed (**Fig. 9A**). Western blot experiments indicate that NLRP-3 and ASC protein levels were relatively stable in all tested conditions (**Fig. 9B**). However, the protein expression of pro-IL-1β was undetectable in caspase-4 deficient cells even if primed with LPS, a known NLRP-3 inflammasome primer (35). $AgNP_{15}$ was found to induce cleavage of caspase-1 and apparition of the p20 caspase-1 fragment in both control and caspase-4-deficient cells primed with LPS. Despite the fact that $AgNP_{15}$ induced an increase caspase-1 activity in caspase-4 deficient cells (**Fig. 9C**), the IL-1β secretion was decreased in caspase-4 deficient cells vs the corresponding control (**Fig. 9D**). In addition, a significant higher proportion of PI-positive cells was observed in caspase-4 deficient cells (**Fig. 9E**), classically used to identify pyroptotic cells (reviewed in (33)). Finally, caspase-4 deficient cells had an increased amount of pyroptosome compared to control cells (**Fig. 9F**). These results suggested that caspase-4 is essential for priming of the NLRP-3 inflammasome component pro-IL-1β, but would regulate negatively its activation by $AgNP_{15}$.

ATF-6 degradation leads to inflammasome activation and pyroptosis cell death - Because $AgNP_{15}$ induce ER stress events accompanied by a rapid degradation of the ATF-6 sensor, we next determined whether or not this pathway could regulate the activation of the NLRP-3 inflammasome. To do so, we have used specific inhibitors of S1P and S2P, two proteases involved in ATF-6 cleavage (7). We first evaluated the efficiency of the two inhibitors of PF-429242 (S1P inhibitor) and 1,10-phenanthroline (S2P inhibitor) on processing of one of their main substrate, SREBP-1. 1,10- phenanthroline stongly inhibited the processing of SREBP-1 while PF-429242 did not appear to block its degradation. Of note, $AgNP_{15}$ alone reduced its processing. Pre-treatment of the cells with PF-429242, reduced moderately $AgNP_{15}$-induced ATF-6 processing into its active fragment, but the use of 1,10-phenanthroline was found to drastically prevent its processing and apparition of its cleaved fragment (**Fig. 10A**). The effect of $AgNP_{15}$ was similar to the ER-stressor tunicamycin, which alone induced processing of ATF-6, but after 6h of stimulation (**Fig. 10B**). In addition, ATF-6 processing correlated with increased caspase-1 processing and activity (**Fig. 10C**) as well as with IL-1β secretion (**Fig. 10D**) and the % of PI-positive cells (**Fig. 10E)**, suggesting an important role for ATF-6 in the control of pyroptosis. Importantly, treatment with the S2P inhibitor led to a reduction in caspase-1 activity, IL-1β secretion and % of PI-positive cells. These results suggest a possible link between ATF-6 degradation and induction of pyroptosis cell death.

$AgNP_{15}$ induce activation of the inflammasome in primary human monocytes and macrophages

We then wanted to compare the effect of $AgNP_{15}$ on activation of the NLRP-3 inflammasome in primary human monocyte and macrophage cells. Expression of pro-IL-1β and NLRP-3 was clearly different in primary monocytes and macrophages compared to THP-1 cells. Indeed, expression of pro-IL-1β was undetectable in THP-1 cells and macrophages while we observed a basal level in monocytes. Moreover, NLRP-3 expression in THP-1 cells remained similar even after 6h of priming while its expression in monocytes and macrophages increased overtime after 3-6h of stimulation with LPS (**Fig. 11A)**. Secretion of mature IL-1β was also quantified in these three cell types in response to $AgNP_{15}$. Priming with LPS alone was sufficient to induce the secretion of IL-1β in THP-1 and macrophages (**Fig. 11B)**. Conversely, treatment with $AgNP_{15}$ alone, without LPS-priming, led to a significant production of IL-1β in primary monocytes, suggesting that these cells respond differently than THP-1 and macrophages. However in these three cell types, priming with LPS followed by stimulation with $AgNP_{15}$ induced the strongest response.

DISCUSSION

AgNPs are gaining increasing attention as utilization of these NPs are becoming more and more important in a plethora of medical products (36) and, therefore, increase potential human exposure, raising important toxicological considerations. In this study, we provide new evidences for a potential cytotoxic role of $AgNP_{15}$, as demonstrated by activation of ER stress events accompanied by the activation of the NLRP-3 inflammasome and pyroptosis. Different types of nanoparticles were shown to induce ER stress response, including zinc oxide (37). However, only a few studies reported that AgNPs can induce ER stress events in zebrafish and in human Chang liver cells (11,12).

Accumulation of unfolded proteins in the ER leads to transition of ATF-6, where it is processed by S1P and S2P (7). Results of the present study indicate that 25 µg/mL $AgNP_{15}$ induce rapid processing of ATF-6 (within 1h) in human monocytes, an effect not observed at lower concentrations. Interestingly, activation of the NLRP-3 inflammasome was also only induced in response to stimulation with 25 µg/mL $AgNP_{15}$, suggesting that ATF-6 could act as a molecular switch to induce the activation of this inflammasome. Indeed, inhibition of S2P (and S1P, to a lower extend), blocked not only ATF-6 processing, but also activation of the inflammasome. Our results are in agreement with others reporting that inhibition of S2P was more efficient than S1P to block processing of ATF-6 (38,39). Interestingly, a recent study demonstrated that the classical ER stressor, tunicamycin, is sufficient for the induction of IL-1β, suggesting a possible link between ER stress and the inflammasome (40). Moreover, tunicamycin was previously shown to induce ATF-6 degradation (7). Another report also demonstrates that inhibition ER stress by sodium 4-phenylbutyrate results in a significant reduction in IL-1β levels, supporting the role of ER stress in IL-1β production (41). However, to the best of our knowledge, the role of ATF-6 in the activation of the NLRP-3 inflammasome had never been investigated before.

The inflammasomes are multiprotein complexes activated upon cytosolic perturbations such as cellular infection (17,32). This complex mediates the activation of the inflammatory caspase-1 which is critical for the secretion of mature IL-1β and formation of pores at the cell membrane (42). Multiple inflammasomes have been characterized including NLRC-4, AIM-2 and NLRP-3. Among them, NLRP-3 is the one that has been more studied and known to be activated upon various type of stimuli, including asbestos, silica, uric acid and ATP (43-45). Conversely to the NLRC-4 or the AIM-2, the NLRP-3 inflammasome is controlled by a priming step that requires de novo protein translation (35). Although carbon nanotubes and carbon black have also been reported to activate this inflammasome in THP-1 and murine bone marrow-derived cells (20,46), the effect of AgNPs on the inflammasome has never been reported. Herein, we show a cytotoxic and inflammatory role of $AgNP_{15}$ as evidenced by induction of pyroptosis cell death and IL-1β secretion. Indeed, $AgNP_{15}$-treated cells harbored the characteristics of pyroptotic cell death: increased processing and activity of caspase-1, pyroptosome formation, loss of membrane integrity and secretion of IL-1β. The experiments on THP-1, primary monocytes and macrophages also provide new mechanisms of action of the regulation of the NLRP-3 inflammasome. For instance, the basal expression level of the different components of this pathway were found to be slightly different in THP-1, primary monocytes and macrophages. This resulted in a significant variation in the amount of mature IL-1β secreted within the extracellular space. Indeed, $AgNP_{15}$-treated primary monocytes secreted significant amount of IL-1β without the priming of LPS. Of note, we could detect a significant expression level of NLRP-3 and pro-IL-1β in resting monocytes, possibly explaining the secretion of IL-1β in $AgNP_{15}$-treated cells.

Secretion of IL-1β is associated with acute inflammation and pathogenesis of multiple chronic inflammatory diseases (16) fitting well with previous studies indicating that nanosilver possess some toxic and proinflammatory effects (47-50). However, in a subacute murine inhalation model, some authors reported that AgNPs induces minimal lung toxicity or inflammation (51). These

observations explain why some authors are interested in trying to answer if AgNPs are allies or adversaries (52). Therefore, the results of the present study are in line with the need to further study the mechanisms of the action of AgNPs on mammalian cells at the molecular level, in order to assure a safe application of AgNPs.

Althought we provide new evidences in the toxicity of AgNPs, the exact mechanisms underlying the effects of $AgNP_{15}$ still remains to be clarified. Even if we clearly observed $AgNP_{15}$ inside cells, particularly close to or in the nucleus, we cannot definitely conclude that AgNPs have to penetrate cells to exert biological effects. Based on the internalization inhibitory experiments, we may speculate that internalization of $AgNP_{15}$ might be dispensable for its effects on IL-1β secretion. Morever, the effect of $AgNP_{15}$ was clearly dependent on caspase-1 as inhibition of this protein resulted in abolition of IL-1β secretion. Furthermore, although we observed ATF6 degradation in response to $AgNP_{15}$, it cannot be ruled out that silver ions are somewhat involved. However, it is important to specify that we have used a commercial source of AgNPs and we have used them as is, as they are probably used in different applications. Our results also indicate that the processing of ATF-6 and the apparition of the cleaved fragment correlate with the increased expression of caspase-1 p20, caspase-1 activity, IL-1β secretion and the % of PI-positive cells, supporting inflammasome activation. Through inhibition of ATF-6 processing, we clearly see a reduction in caspase-1 activity, IL-1β secretion and the % of PI-positive cells, suggesting that ATF-6 degradation is a related event to activation of the NLRP-3 inflammasome and pyroptosis cell death. It is noteworthy that this effect was clearly different than apoptosis cell death.

Caspase-4 belongs to the human inflammatory caspase family along with caspase-1, -5 and -12 (53). The involvement of caspase-4 in ER stress has been previously established (25,27) but has also been recently challenged (34,54). Nevertheless, to date, only a few studies reported potential involvement of caspase-4 in the activation of the inflammasomes (30,55). Our results indicate that caspase-4 is indeed required for the priming of the inflammasome, as absence of this caspase resulted in a severe impairment of pro-IL-1β synthesis. However, absence of caspase-4 also resulted in a significant increase in the activity of active caspase-1 and the proportion of PI-positive and pyroptosome-positive cells. These results suggest that caspase-4 would therefore regulate negatively the NLRP-3 inflammasome activation but would play an important role in its priming step. It is noteworthy that, in caspase-4 deficient THP-1 cells, the NF-κB pathway is markedly affected, since caspase-4 was previously found to interact with TRAF-6, agreeing with the lack of pro-IL-1β in these cells (22). In another study, IL-1β production was found to be dependent on NF-κB in THP-1 cells (56). Putting this information with the fact that priming of the inflammasomes is dependent of NF-κB activation and that caspase-4 deficient cells have reduced NF-κB transduction, is in agreement with our observation on the impairment of pro-IL-1β in caspase-4 deficient cells. Because we make our observations at a concentration of 25 µg/ml $AgNP_{15}$, and not at 1-10 µg/ml, it would be of interest in future to establish if the same would be true for AgNPs with a different starting diameter, since this variable is highly important in the induction of different biological effects previously reported for cell toxicity of AgNPs in bacteria, yeast, algae, crustaceans and mammalian cells in vitro (57). Because of the great potential and interest that AgNPs represent for developing future therapies based on drug delivery, further studied need to be conducted in order to limit undesired potential effect of AgNPs.

REFERENCES

1. Kim, J., Kuk, E., Yu, K., Kim, J., Park, S., Lee, H., Kim, S., Park, Y., Park, Y., Hwang, C.-Y., Kim, Y., Lee, Y., Jeong, D., and Cho, M. (2007) Antimicrobial effects of silver nanoparticles. *Nanomedicine* **3**, 95 - 101
2. Slawson, R., Trevors, J., and Lee, H. (1992) Silver accumulation and resistance in Pseudomonas stutzeri. *Arch. Microbiol.* **158**, 398 - 404
3. Sondi, I., and Salopek-Sondi, B. (2004) Silver nanoparticles as antimicrobial agent: a case study on E. coli as a model for Gram-negative bacteria. *J. Colloid Interface Sci.* **275**, 177 - 182
4. Bertolotti, A., Zhang, Y., Hendershot, L. M., Harding, H. P., and Ron, D. (2000) Dynamic interaction of BiP and ER stress transducers in the unfolded-protein response. *Nat Cell Biol* **2**, 326-332
5. Liu, C. Y., Schroder, M., and Kaufman, R. J. (2000) Ligand-independent dimerization activates the stress response kinases IRE1 and PERK in the lumen of the endoplasmic reticulum. *J Biol Chem* **275**, 24881-24885
6. Harding, H. P., Zhang, Y., and Ron, D. (1999) Protein translation and folding are coupled by an endoplasmic-reticulum-resident kinase. *Nature* **397**, 271-274
7. Ye, J., Rawson, R. B., Komuro, R., Chen, X., Dave, U. P., Prywes, R., Brown, M. S., and Goldstein, J. L. (2000) ER stress induces cleavage of membrane-bound ATF6 by the same proteases that process SREBPs. *Mol Cell* **6**, 1355-1364
8. Yoshida, H., Matsui, T., Yamamoto, A., Okada, T., and Mori, K. (2001) XBP1 mRNA is induced by ATF6 and spliced by IRE1 in response to ER stress to produce a highly active transcription factor. *Cell* **107**, 881-891
9. Lin, J. H., Li, H., Yasumura, D., Cohen, H. R., Zhang, C., Panning, B., Shokat, K. M., Lavail, M. M., and Walter, P. (2007) IRE1 signaling affects cell fate during the unfolded protein response. *Science* **318**, 944-949
10. Chen, R., Huo, L., Shi, X., Bai, R., Zhang, Z., Zhao, Y., Chang, Y., and Chen, C. (2014) Endoplasmic Reticulum Stress Induced by Zinc Oxide Nanoparticles Is an Earlier Biomarker for Nanotoxicological Evaluation. *ACS nano*
11. Zhang, R., Piao, M. J., Kim, K. C., Kim, A. D., Choi, J. Y., Choi, J., and Hyun, J. W. (2012) Endoplasmic reticulum stress signaling is involved in silver nanoparticles-induced apoptosis. *Int J Biochem Cell Biol* **44**, 224-232
12. Christen, V., Capelle, M., and Fent, K. (2013) Silver nanoparticles induce endoplasmatic reticulum stress response in zebrafish. *Toxicol Appl Pharmacol* **272**, 519-528
13. Labbé, K., and Saleh, M. (2011) Pyroptosis: A Caspase-1-Dependent Programmed Cell Death and a Barrier to Infection. in *The Inflammasomes* (Couillin, I., Pétrilli, V., and Martinon, F. eds.), Springer Basel. pp 17-36
14. Fernandes-Alnemri, T., Wu, J., Yu, J. W., Datta, P., Miller, B., Jankowski, W., Rosenberg, S., Zhang, J., and Alnemri, E. S. (2007) The pyroptosome: a supramolecular assembly of ASC dimers mediating inflammatory cell death via caspase-1 activation. *Cell Death Differ* **14**, 1590-1604
15. Dinarello, C. A. (2009) Immunological and inflammatory functions of the interleukin-1 family. *Annu Rev Immunol* **27**, 519-550
16. Dinarello, C. A. (2011) Interleukin-1 in the pathogenesis and treatment of inflammatory diseases. *Blood* **117**, 3720-3732
17. Franchi, L., Eigenbrod, T., Munoz-Planillo, R., and Nunez, G. (2009) The inflammasome: a caspase-1-activation platform that regulates immune responses and disease pathogenesis. *Nat Immunol* **10**, 241-247
18. Meunier, E., Coste, A., Olagnier, D., Authier, H., Lefevre, L., Dardenne, C., Bernad, J., Beraud, M., Flahaut, E., and Pipy, B. (2012) Double-walled carbon nanotubes trigger IL-1beta release in human monocytes through Nlrp3 inflammasome activation. *Nanomedicine* **8**, 987-995

19. Yang, E. J., Kim, S., Kim, J. S., and Choi, I. H. (2012) Inflammasome formation and IL-1beta release by human blood monocytes in response to silver nanoparticles. *Biomaterials* **33**, 6858-6867
20. Reisetter, A. C., Stebounova, L. V., Baltrusaitis, J., Powers, L., Gupta, A., Grassian, V. H., and Monick, M. M. (2011) Induction of inflammasome-dependent pyroptosis by carbon black nanoparticles. *J Biol Chem* **286**, 21844-21852
21. Poirier, M., Simard, J. C., Antoine, F., and Girard, D. (2014) Interaction between silver nanoparticles of 20 nm (AgNP20) and human neutrophils: induction of apoptosis and inhibition of de novo protein synthesis by AgNP20 aggregates. *Journal of applied toxicology : JAT* **34**, 404-412
22. Lakshmanan, U., and Porter, A. G. (2007) Caspase-4 interacts with TNF receptor-associated factor 6 and mediates lipopolysaccharide-induced NF-kappaB-dependent production of IL-8 and CC chemokine ligand 4 (macrophage-inflammatory protein-1). *J Immunol* **179**, 8480-8490
23. Vallieres, F., and Girard, D. (2013) IL-21 enhances phagocytosis in mononuclear phagocyte cells: identification of spleen tyrosine kinase as a novel molecular target of IL-21. *J Immunol* **190**, 2904-2912
24. Simard, J. C., Cesaro, A., Chapeton-Montes, J., Tardif, M., Antoine, F., Girard, D., and Tessier, P. A. (2013) S100A8 and S100A9 induce cytokine expression and regulate the NLRP3 inflammasome via ROS-dependent activation of NF-kappaB(1.). *PLoS One* **8**, e72138
25. Binet, F., Chiasson, S., and Girard, D. (2010) Evidence that endoplasmic reticulum (ER) stress and caspase-4 activation occur in human neutrophils. *Biochem Biophys Res Commun* **391**, 18-23
26. Poirier, M., Simard, J. C., Antoine, F., and Girard, D. (2013) Interaction between silver nanoparticles of 20 nm (AgNP) and human neutrophils: induction of apoptosis and inhibition of de novo protein synthesis by AgNP aggregates. *Journal of applied toxicology : JAT*
27. Hitomi, J., Katayama, T., Eguchi, Y., Kudo, T., Taniguchi, M., Koyama, Y., Manabe, T., Yamagishi, S., Bando, Y., Imaizumi, K., Tsujimoto, Y., and Tohyama, M. (2004) Involvement of caspase-4 in endoplasmic reticulum stress-induced apoptosis and Abeta-induced cell death. *The Journal of cell biology* **165**, 347-356
28. Edamatsu, T., Xiao, Y. Q., Tanabe, J., Mue, S., and Ohuchi, K. (1997) Induction of neutrophil chemotactic factor production by staurosporine in rat peritoneal neutrophils. *Br J Pharmacol* **121**, 1651-1658
29. Labbe, K., and Saleh, M. (2008) Cell death in the host response to infection. *Cell Death Differ* **15**, 1339-1349
30. Sollberger, G., Strittmatter, G. E., Kistowska, M., French, L. E., and Beer, H. D. (2012) Caspase-4 is required for activation of inflammasomes. *J Immunol* **188**, 1992-2000
31. Akhtar, M. J., Ahamed, M., Alhadlaq, H. A., Alrokayan, S. A., and Kumar, S. (2014) Targeted anticancer therapy: Overexpressed receptors and nanotechnology. *Clin Chim Acta*
32. Schroder, K., and Tschopp, J. (2010) The inflammasomes. *Cell* **140**, 821-832
33. Miao, E. A., Rajan, J. V., and Aderem, A. (2011) Caspase-1-induced pyroptotic cell death. *Immunol Rev* **243**, 206-214
34. Binet, F., Chiasson, S., and Girard, D. (2010) Arsenic trioxide induces endoplasmic reticulum stress-related events in neutrophils. *Int Immunopharmacol* **10**, 508-512
35. Bauernfeind, F. G., Horvath, G., Stutz, A., Alnemri, E. S., MacDonald, K., Speert, D., Fernandes-Alnemri, T., Wu, J., Monks, B. G., Fitzgerald, K. A., Hornung, V., and Latz, E. (2009) Cutting edge: NF-kappaB activating pattern recognition and cytokine receptors license NLRP3 inflammasome activation by regulating NLRP3 expression. *J Immunol* **183**, 787-791
36. Nowack, B., Krug, H. F., and Height, M. (2011) 120 Years of Nanosilver History: Implications for Policy Makers. *Environ Sci Technol* **10**, 10
37. Chen, R., Huo, L., Shi, X., Bai, R., Zhang, Z., Zhao, Y., Chang, Y., and Chen, C. (2014) Endoplasmic reticulum stress induced by zinc oxide nanoparticles is an earlier biomarker for nanotoxicological evaluation. *ACS Nano* **8**, 2562-2574

38. Guan, M., Fousek, K., and Chow, W. A. (2012) Nelfinavir inhibits regulated intramembrane proteolysis of sterol regulatory element binding protein-1 and activating transcription factor 6 in castration-resistant prostate cancer. *The FEBS journal* **279**, 2399-2411
39. Guan, M., Fousek, K., Jiang, C., Guo, S., Synold, T., Xi, B., Shih, C. C., and Chow, W. A. (2011) Nelfinavir induces liposarcoma apoptosis through inhibition of regulated intramembrane proteolysis of SREBP-1 and ATF6. *Clinical cancer research : an official journal of the American Association for Cancer Research* **17**, 1796-1806
40. Kim, S., Joe, Y., Jeong, S. O., Zheng, M., Back, S. H., Park, S. W., Ryter, S. W., and Chung, H. T. (2013) Endoplasmic reticulum stress is sufficient for the induction of IL-1beta production via activation of the NF-kappaB and inflammasome pathways. *Innate immunity*
41. Kim, H. J., Jeong, J. S., Kim, S. R., Park, S. Y., Chae, H. J., and Lee, Y. C. (2013) Inhibition of endoplasmic reticulum stress alleviates lipopolysaccharide-induced lung inflammation through modulation of NF-kappaB/HIF-1alpha signaling pathway. *Scientific reports* **3**, 1142
42. Fink, S. L., and Cookson, B. T. (2006) Caspase-1-dependent pore formation during pyroptosis leads to osmotic lysis of infected host macrophages. *Cell Microbiol* **8**, 1812-1825
43. Martinon, F., Petrilli, V., Mayor, A., Tardivel, A., and Tschopp, J. (2006) Gout-associated uric acid crystals activate the NALP3 inflammasome. *Nature* **440**, 237-241
44. Dostert, C., Petrilli, V., Van Bruggen, R., Steele, C., Mossman, B. T., and Tschopp, J. (2008) Innate immune activation through Nalp3 inflammasome sensing of asbestos and silica. *Science* **320**, 674-677
45. Kahlenberg, J. M., Lundberg, K. C., Kertesy, S. B., Qu, Y., and Dubyak, G. R. (2005) Potentiation of caspase-1 activation by the P2X7 receptor is dependent on TLR signals and requires NF-kappaB-driven protein synthesis. *J Immunol* **175**, 7611-7622
46. Yang, M., Flavin, K., Kopf, I., Radics, G., Hearnden, C. H., McManus, G. J., Moran, B., Villalta-Cerdas, A., Echegoyen, L. A., Giordani, S., and Lavelle, E. C. (2013) Functionalization of carbon nanoparticles modulates inflammatory cell recruitment and NLRP3 inflammasome activation. *Small* **9**, 4194-4206
47. Kanapathipillai, M., Brock, A., and Ingber, D. E. *Nanoparticle targeting of anti-cancer drugs that alter intracellular signaling or influence the tumor microenvironment*, Adv Drug Deliv Rev. 2014 May 9. pii: S0169-409X(14)00099-4. doi: 10.1016/j.addr.2014.05.005.
48. Lohcharoenkal, W., Wang, L., Chen, Y. C., and Rojanasakul, Y. (2014) Protein nanoparticles as drug delivery carriers for cancer therapy. *Biomed Res Int* **180549**, 20
49. Chen, X., and Schluesener, H. J. (2008) Nanosilver: a nanoproduct in medical application. *Toxicol Lett* **176**, 1-12
50. Kulthong, K., Srisung, S., Boonpavanitchakul, K., Kangwansupamonkon, W., and Maniratanachote, R. (2010) Determination of silver nanoparticle release from antibacterial fabrics into artificial sweat. *Part Fibre Toxicol* **7**, 1743-8977
51. Stebounova, L. V., Adamcakova-Dodd, A., Kim, J. S., Park, H., O'Shaughnessy, P. T., Grassian, V. H., and Thorne, P. S. (2011) Nanosilver induces minimal lung toxicity or inflammation in a subacute murine inhalation model. *Part Fibre Toxicol* **8**, 1743-8977
52. Bartlomiejczyk, T., Lankoff, A., Kruszewski, M., and Szumiel, I. (2013) Silver nanoparticles -- allies or adversaries? *Annals of agricultural and environmental medicine : AAEM* **20**, 48-54
53. McIlwain, D. R., Berger, T., and Mak, T. W. (2013) Caspase functions in cell death and disease. *Cold Spring Harbor perspectives in biology* **5**, a008656
54. Obeng, E. A., and Boise, L. H. (2005) Caspase-12 and caspase-4 are not required for caspase-dependent endoplasmic reticulum stress-induced apoptosis. *J Biol Chem* **280**, 29578-29587
55. Kajiwara, Y., Schiff, T., Voloudakis, G., Gama Sosa, M. A., Elder, G., Bozdagi, O., and Buxbaum, J. D. (2014) A critical role for human caspase-4 in endotoxin sensitivity. *J Immunol* **193**, 335-343

56. Yallapu, M. M., Gupta, B. K., Jaggi, M., and Chauhan, S. C. (2010) Fabrication of curcumin encapsulated PLGA nanoparticles for improved therapeutic effects in metastatic cancer cells. *J Colloid Interface Sci* **351**, 19-29
57. Ivask, A., Kurvet, I., Kasemets, K., Blinova, I., Aruoja, V., Suppi, S., Vija, H., Kakinen, A., Titma, T., Heinlaan, M., Visnapuu, M., Koller, D., Kisand, V., and Kahru, A. (2014) Size-dependent toxicity of silver nanoparticles to bacteria, yeast, algae, crustaceans and Mammalian cells in vitro. *PLoS One* **9**

TABLES

Table 1. Characterization of $AgNP_{15}$ by dynamic light scattering.

FIGURE LEGENDS

FIGURE 1. *Transmission electronic microscopy image of the primary stock solution of $AgNP_{15}$ and behavior of the nanoparticle under different concentrations in culture medium evaluated by DLS analysis.* (A) Sample of the solution stock from the manufacturer was used for characterization by transmission electronic microscopy illustrating that the suspension was relatively homogeneous with the majority of AgNPs with a diameter close to 15 nm, but also others with different smaller and greater diameters. (B) Representative data obtained by DLS analysis performed at 37 ^{o}C with a concentration of 1, 5, 10 or 25 µg/ml $AgNP_{15}$ in RPMI-1640 supplemented with 10% FBS, the experimental conditions used in this study. Data are from one representative experiment out of three.

FIGURE 2. *$AgNP_{15}$ alter the morphology of human monocyte THP-1 cells.* Cells were treated for 24h with buffer (a,g), 1 µM staurosporine (b,h), 1 (c,i), 5 (d,-j), 10 (e,k) or 25 (f,l) µg/mL $AgNP_{15}$. Live cells in plates (A, panels a-f) or cytospin preparations of cells colored with Hema-stained 3 solution (B, panels g-l) were then visualized by optical light microscopy at a magnification of 200X (a-f) or 400X (g-l). Data are from one representative experiment out of three.

FIGURE 3. *Internalization of $AgNP_{15}$ in human monocyte THP-1 cells.* Cells were incubated for 1h with 25 µg/mL $AgNP_{15}$ (A-C), the highest tested concentration, and were visualized by transmission electronic microscopy, as described in the *experimental procedures*. Panel B is an enlarged section of A. Presence of $AgNP_{15}$ large aggregates inside a cytosolic vacuole (black arrows) and small $AgNP_{15}$ aggregates in the cytosol and nucleus (white arrows). Data are from one representative experiment out of three.

FIGURE 4. *$AgNP_{15}$ induce ER stress events in human monocyte THP-1 cells.* ER stress markers were followed by western blot, as described in the *experimental procedures*. Cells were treated for 24h (A) or 1h (B) with 1-25 µg/mL of $AgNP_{15}$, 10 µg/mL of thapsigargin (Tg) or the equivalent volume of buffer (ctrl). Data are from one representative experiment out of three. One example of loading control systematically performed with GAPDH is shown at the bottom of each panel.

FIGURE 5. *$AgNP_{15}$ induce cell death in human monocyte THP-1 cells.* Cell viability was assessed by flow cytometry using Annexin-V-PI staining (A-B). Caspase processing was determined by western blot (C) and caspase activity was quantified using a caspase assay, as described in the *experimental procedures*. Cells were stimulated for 1h (A-B) or 24h (A-C) with buffer (Ctrl), 1-25 µg/mL of $AgNP_{15}$ or 1 µM of staurosporine (Stau). Data are means ± SEM of three (A-B, D-E) or are from one representative experiment out of three (C).

FIGURE 6. *$AgNP_{15}$ induce activation of the inflammasome in human monocyte THP-1 cells*. Cells were treated or not with 100 ng/mL of LPS for 4h and then incubated for 1h with the indicated concentrations of $AgNP_{15}$, 2 mM ATP or buffer (Ctrl). After treatment, the pellets were lysed in Laemmli's buffer for western blot experiments (A) or caspase-1 lysis buffer for caspase-1 assay (B), as described in the *experimental procedures*. For IL-1β quantification, cells were primed 4h with LPS 100 ng/mL (C-D). Cells were then incubated with cytochalasin D (10 µg/mL), dynasore (80 µM) or the equivalent volume of diluent (DMSO) for 30 min before addition of the indicated agonists for 1h (D). Supernatants were harvested to quantify IL-1β by ELISA. Results are from one representative experiment out of three (A) or are expressed as means ± SEM of three independent experiments (B-D).

FIGURE 7. *$AgNP_{15}$ induce pyroptosome assembly in human monocyte THP-1 cells*. Cells were stimulated with 25 µg/mL $AgNP_{15}$, 2mM ATP or buffer (ctrl) for 1h. Cells were then fixed and formation of pyroptosome was followed by confocal microscopy, as described in the *experimental procedures*. Data are from one representative experiment out of three (A) or are expressed as means ± SEM of three independent experiments (B).

FIGURE 8. *NLRP-3 inflammasome activation by $AgNP_{15}$ is dependent on caspase-1 in human monocyte THP-1 cells.* Cells were transfected with siRNA targeting NLRP-3 or non-specific sequence (ctrl) for 24h or 48h (A-C). Protein expression of NLRP-3 was followed by western blot, as described in the *experimental procedures* (A-B). Cells were primed with LPS (100 ng/mL) for 4h, treated or not with 10 µM of YVAD-CHO (D) and then stimulated for 1h with 25 µg/mL $AgNP_{15}$, 2mM ATP or buffer (ctrl). Supernatants were harvested to quantify IL-1β by ELISA. Data are from one representative experiment out of three (A) are expressed as means ± SEM of three independent experiments (B-D).

FIGURE 9. *Role of caspase-4 in the activation of the NLRP-3 inflammasome induced by $AgNP_{15}$ in human monocytes THP-1 cells.* Caspase-4 deficient (TB) or wild type THP-1 cells containing an empty vector (VC) were incubated with buffer or 100 ng/mL LPS for 4h and were then stimulated for 1h with buffer (Ctrl) or 25 µg/ml $AgNP_{15}$). Cell pellets were prepared and lysed in Laemmli's buffer (A-B) for western blot experiments or lysed in caspase-1 lysis buffer for caspase-1 assay (C). For IL-1β quantification, cells were primed 4h with LPS 100 ng/mL before incubation with the indicated agonists. Supernatants were harvested to quantify IL-1β by ELISA (D). Cells were stained with PI for flow cytometry analyzes (E) or with ASC specific antibody for pyroptosome formation (F). Data are from one representative experiment out of three (A-B) or are expressed as means ± SEM of three independent experiments (C-F).

FIGURE 10. *Role of ATF-6 in the activation of the NLRP-3 inflammasome induced by $AgNP_{15}$ in human monocytes.* Cells were pre-incubated with 20 µM of PF-429242 (PF), 500 µM of 1,10-phenanthroline (Phen) or diluent (EtOH) for 30 min and then stimulated for 1h with 25 µg/mL of $AgNP_{15}$ or buffer (Ctrl). tunicamycin (5 µg/mL) treatment for 6h was used as positive control (B). Cells were lysed in Laemmli's buffer (A-B) for western blot experiments, lysed in caspase-1 lysis buffer for caspase-1 assay (C) or stained with PI for flow cytometry analyzes (E). For IL-1β quantification, cells were primed for 4h with 100 ng/mL LPS before incubation with inhibitors and stimulation with the indicated agonists. Supernatants were harvested to perform IL-1β ELISA (D). Data are from one representative experiment out of three (A-B) or are expressed as means ± SEM of three independent experiments(C-E).

FIGURE 11. $AgNP_{15}$ induce secretion of IL-1β in human primary monocytes and macrophages. Cells were primed with LPS (100 ng/mL) for different period of time (A). Protein expression of pro-IL-1β and NLRP-3 was determined by western blot, as described in the *experimental procedures* (A). For IL-1β quantification, cells were primed or not with LPS (100 ng/mL) for 4h and then stimulated for 1h with 25 µg/mL $AgNP_{15}$ or buffer (ctrl). Supernatants were harvested to quantify IL-1β by ELISA. Data are from one representative experiment out of four (A) or are expressed as means ± SEM of five independent experiments (B).

Table 1.

Concentration (µg/mL)	1	5	10	25
Size (nm) (intensity)	66.8 ± 37.5 (69.8% ± 4.4)	86.6 ± 38.8 (79.7% ± 2.0)	54.0 ± 3.2 (85.7% ± 0.7)	64.4 ± 7.3 (93.6 % ± 4.0)
	10.0 ± 0.5 (26.7% ± 3.2)	10.5 ± 2.2 (18.0% ±2.9)	9.1 ± 0.5 (14.3 % ± 0.7)	641.8 ± 1782.0 (5.5% ± 2.8)
	1629.0 ± 2236.0 (3.5% ± 5.3)	2108.0 ±2372.0 (2.4% ± 2.7)		1121.0 ± 2225.0 (0.9% ± 1.7)
Zeta potential (mV)	-8.4 ± 0.3	-9.5 ± 1.0	-8.7 ± 1.2	-9.0 ± 0.7
PdI	0.4 ± 0.3	0.4 ± 0.3	0.2 ± 0.1	0.3 ± 0.1

Results are means from 3-6 different lectures ±SD.
PdI: Polydispersity Index

Figure 1

A

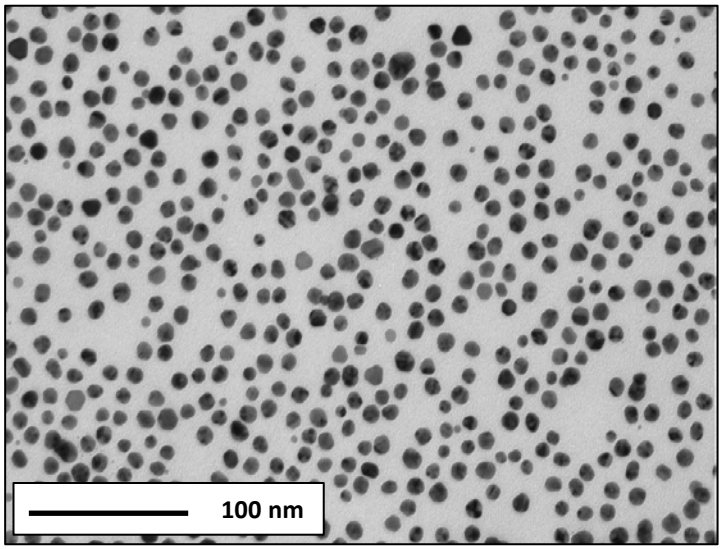

B

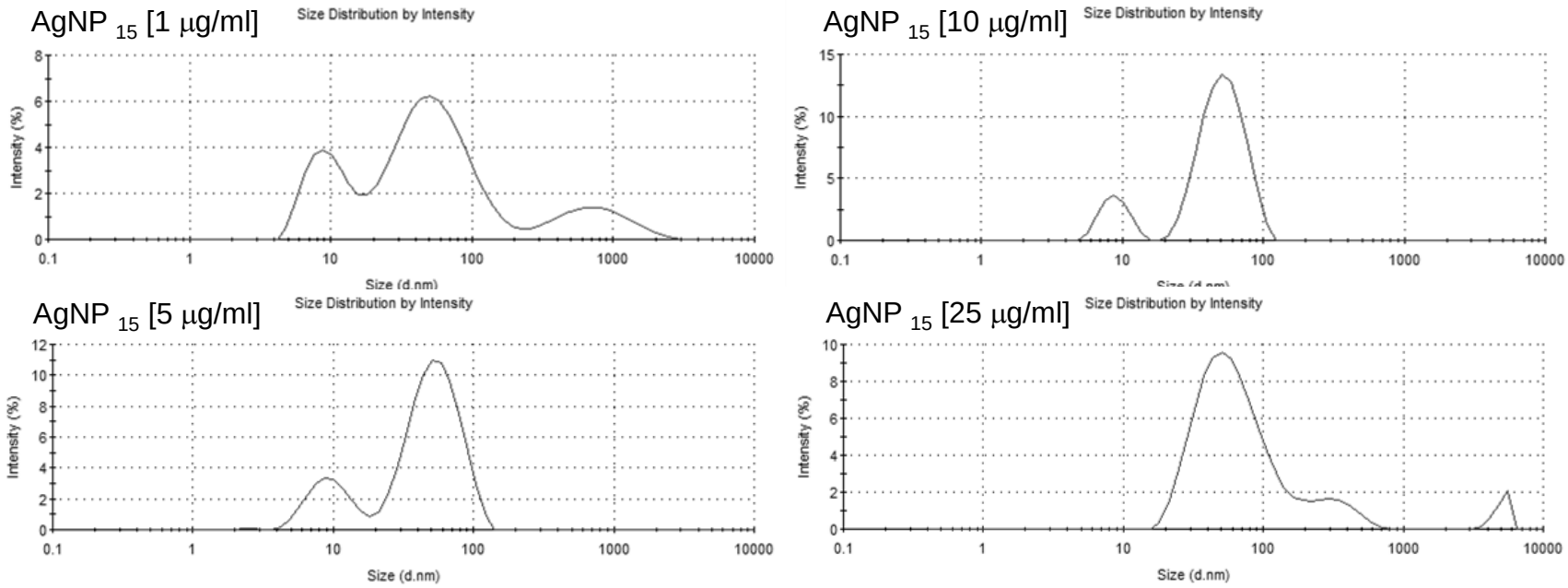

Figure 2

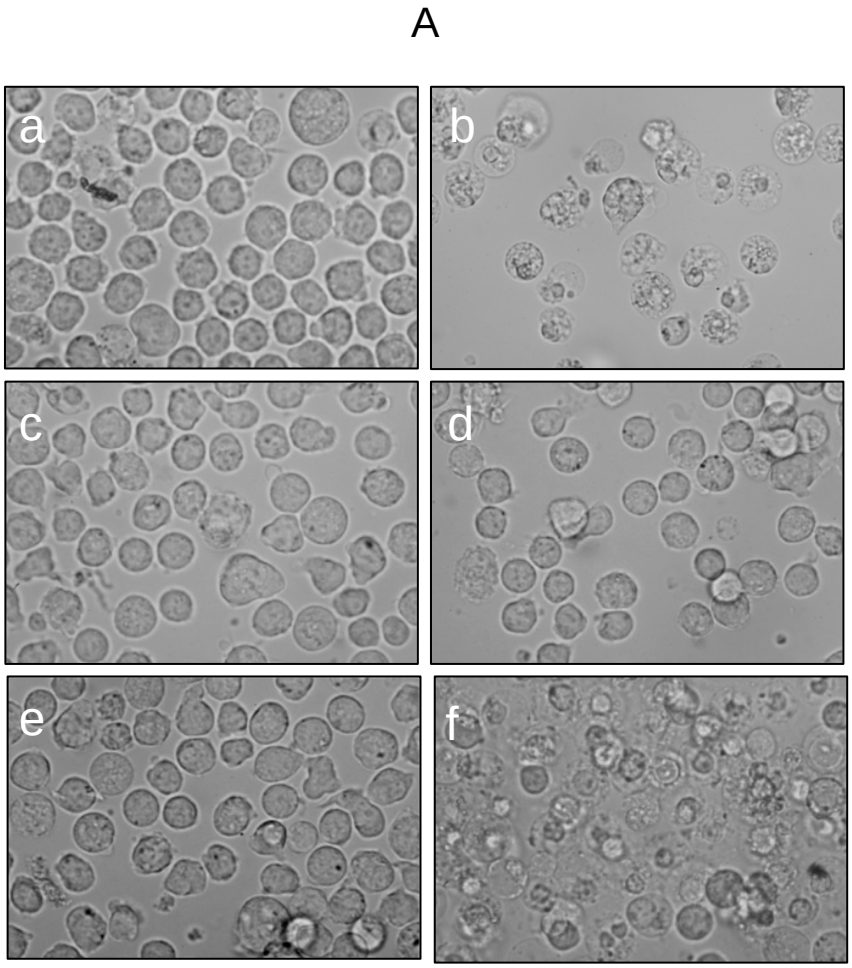

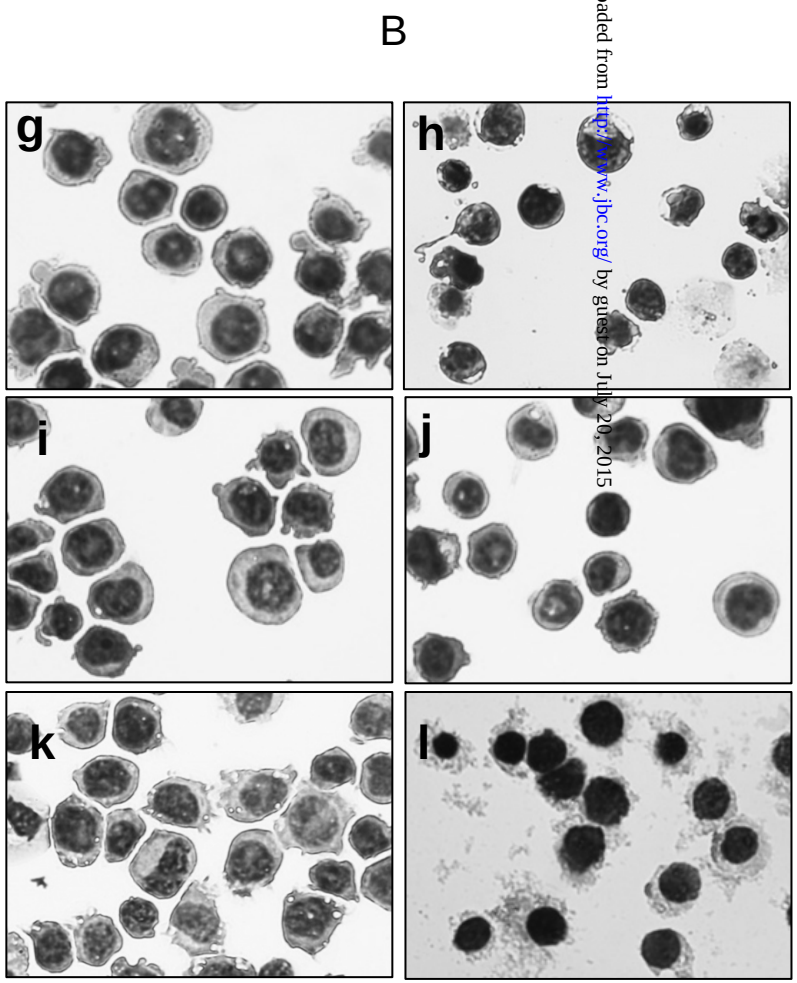

Figure 3

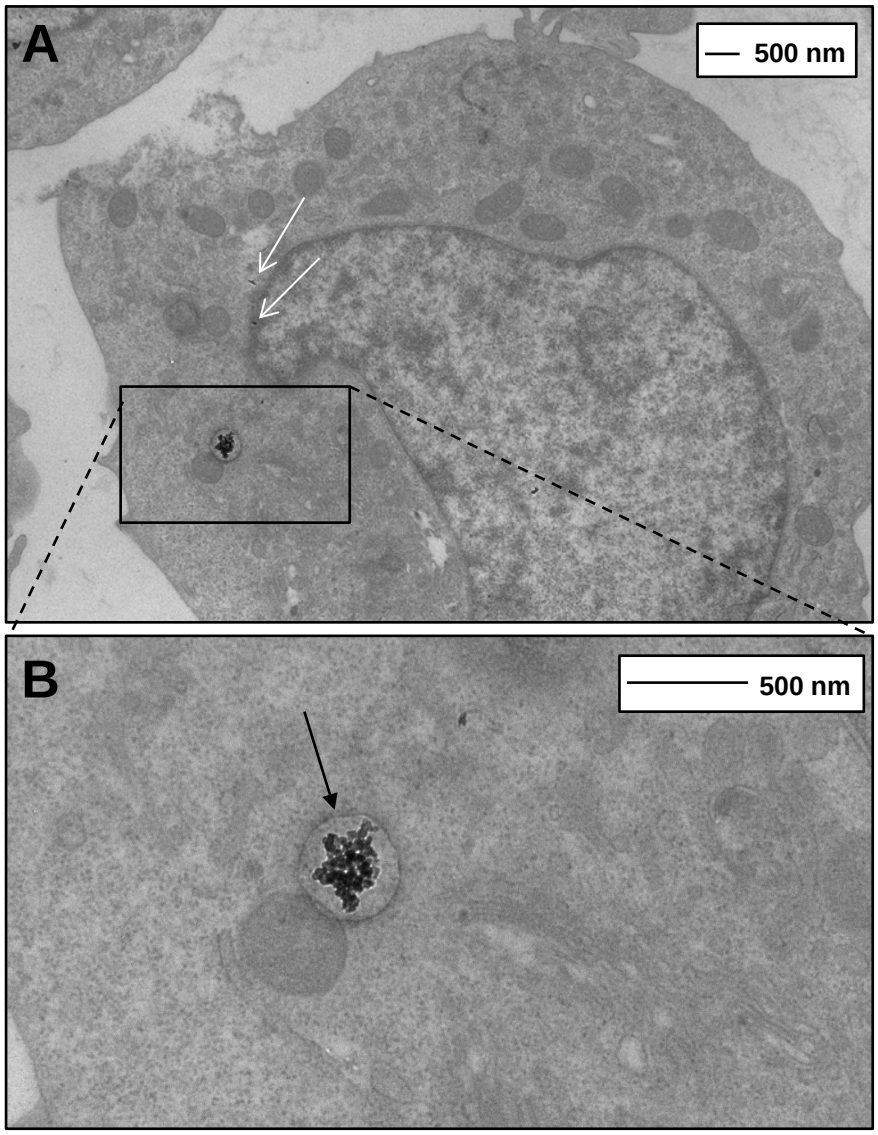

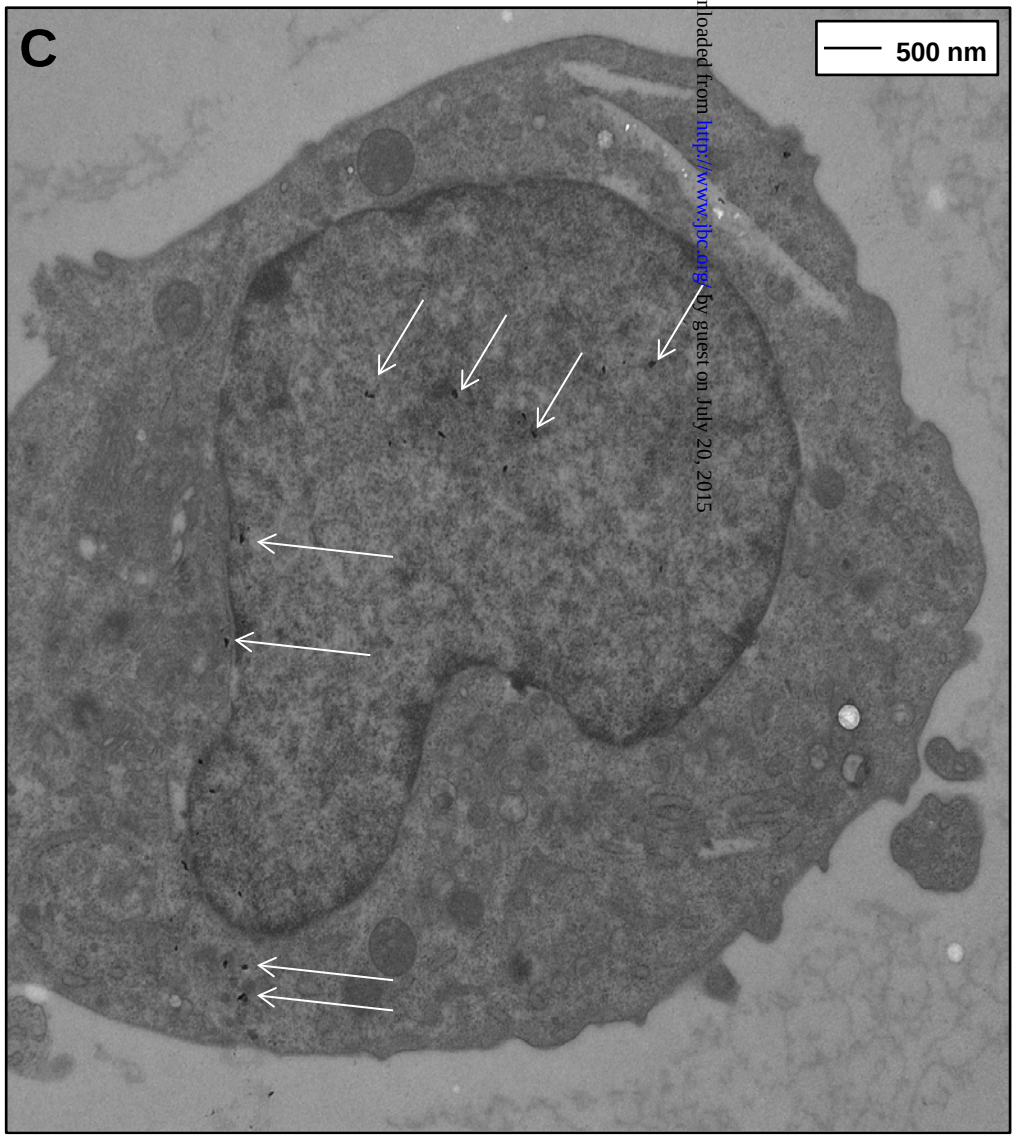

Figure 4

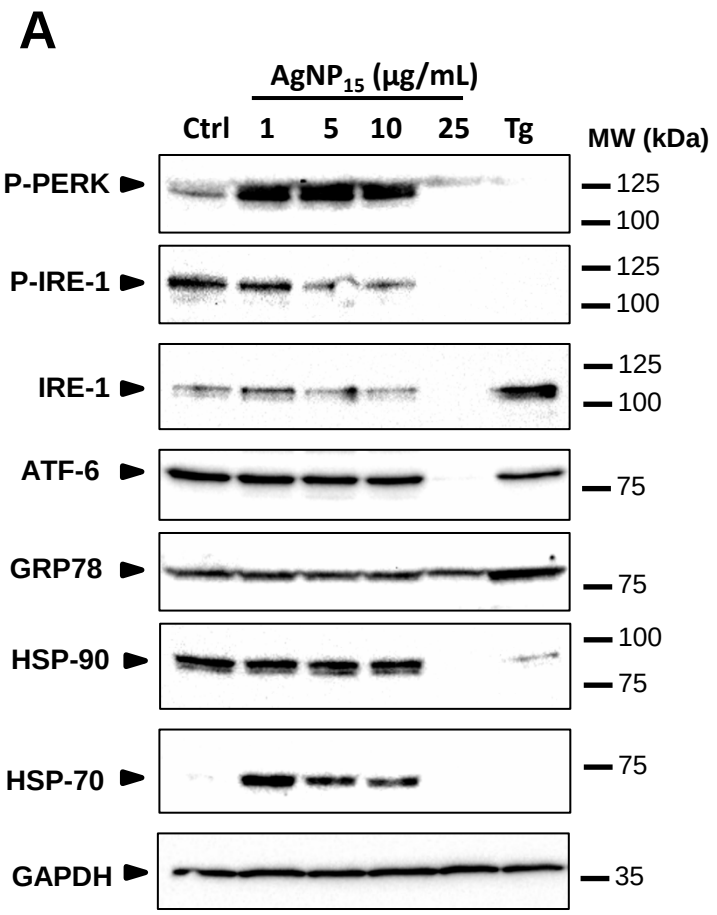

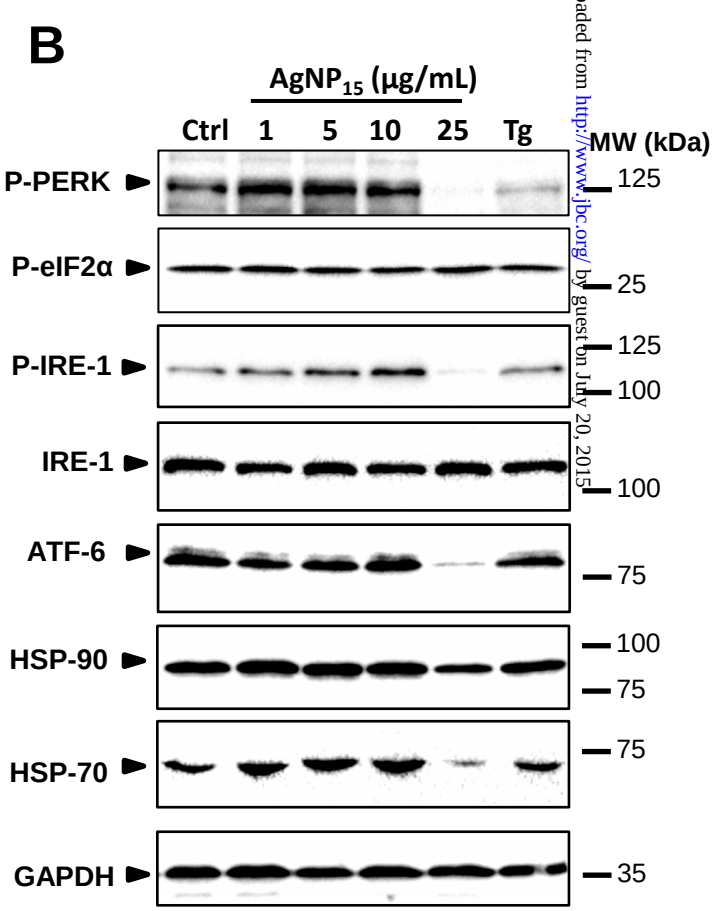

Figure 5

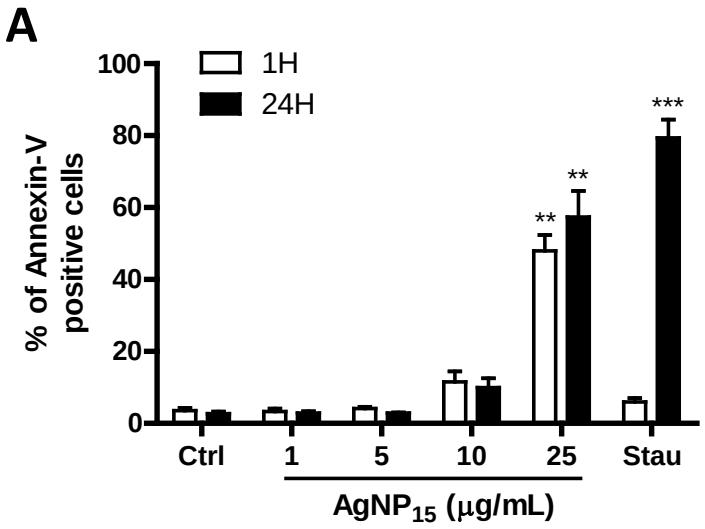

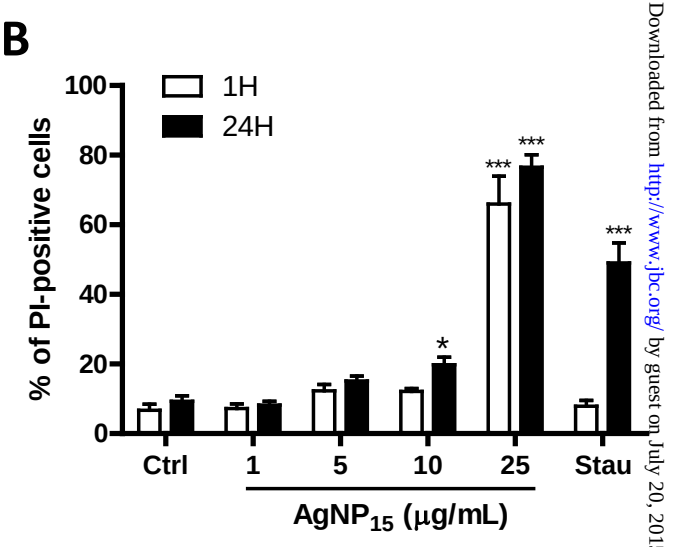

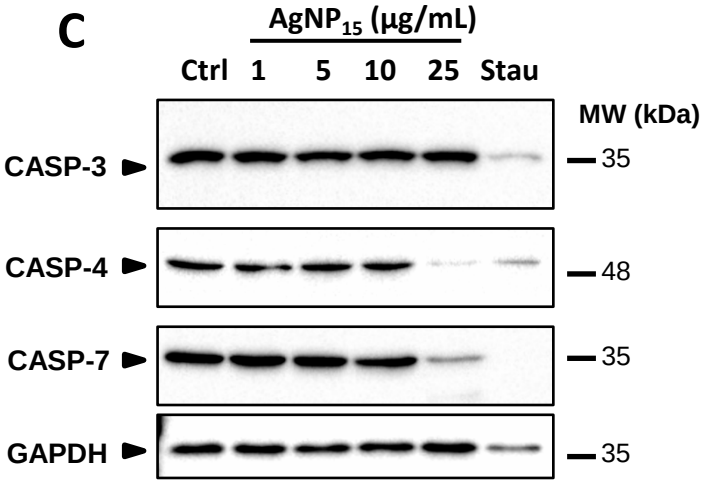

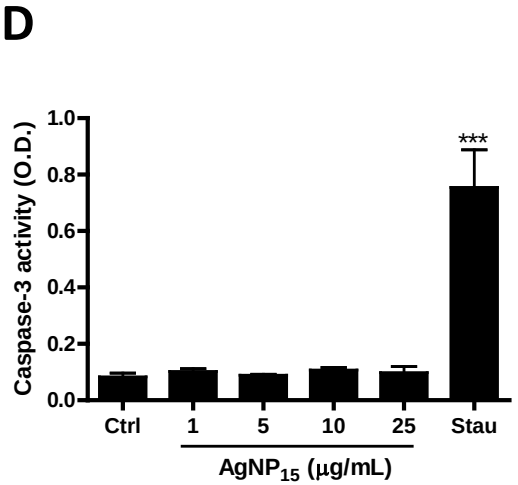

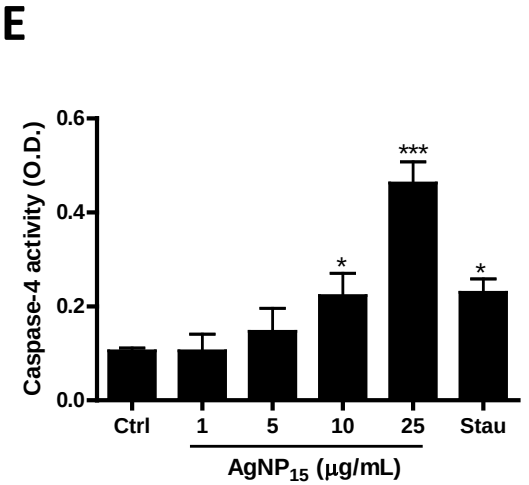

Figure 6

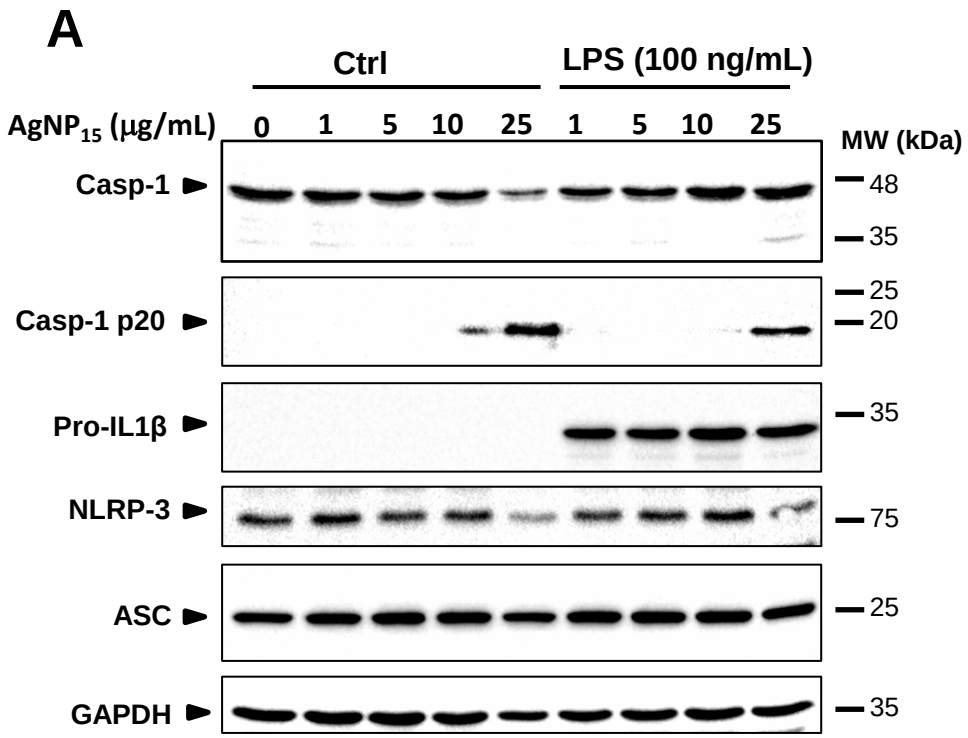

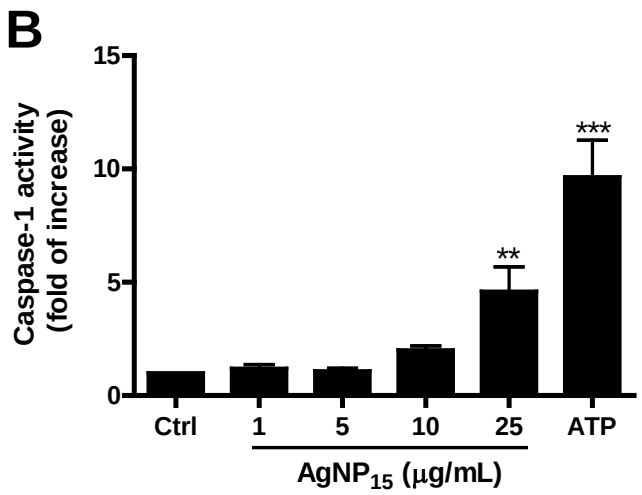

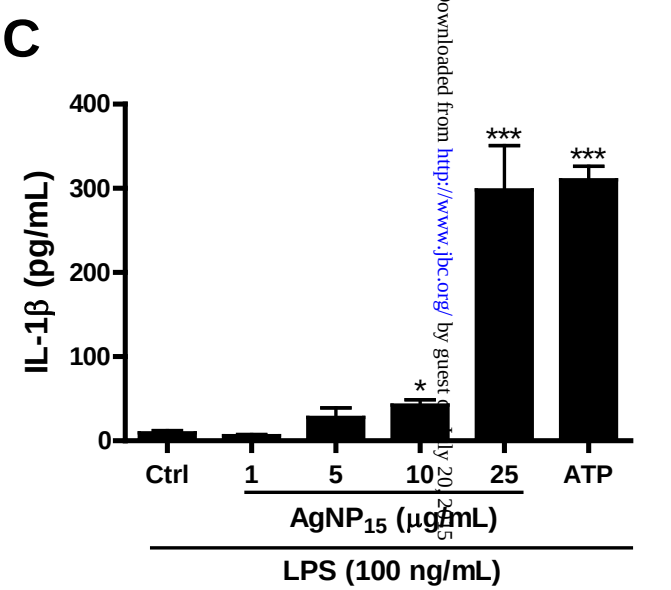

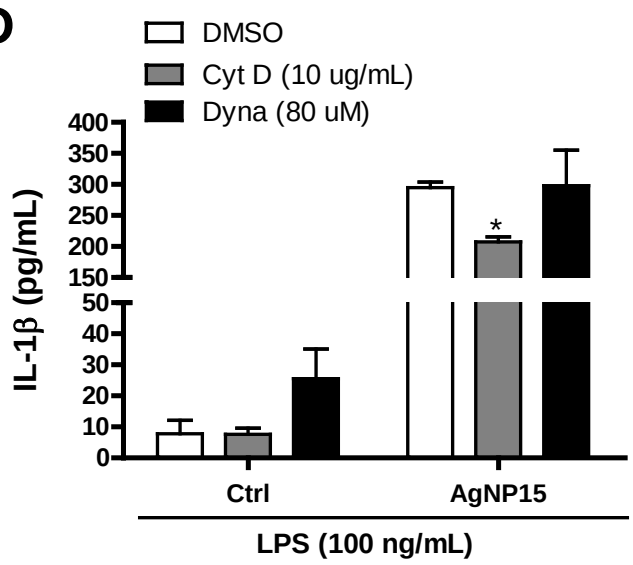

Figure 7

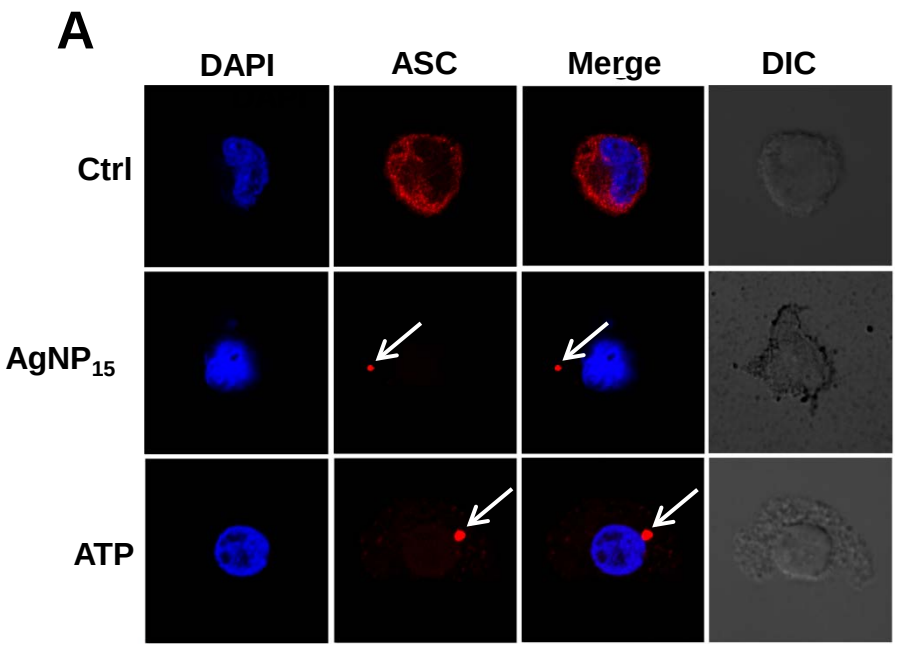

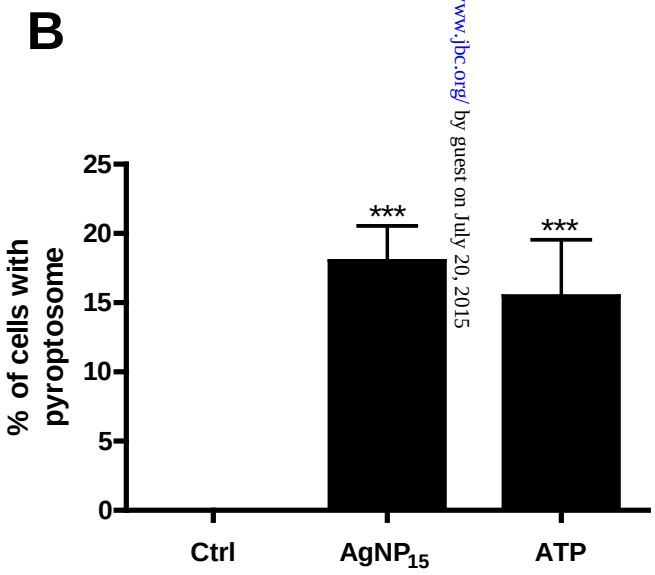

Figure 8

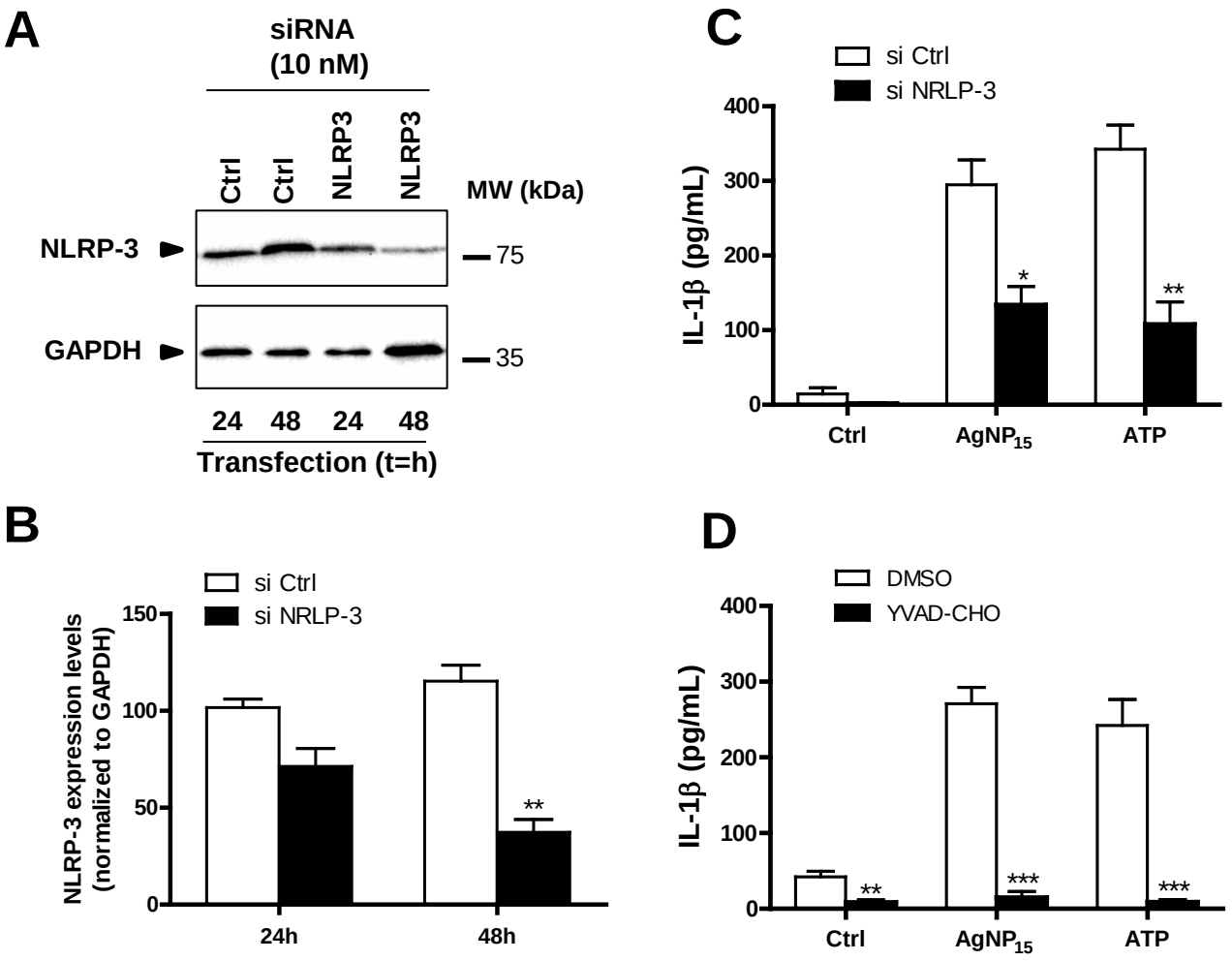

Figure 9

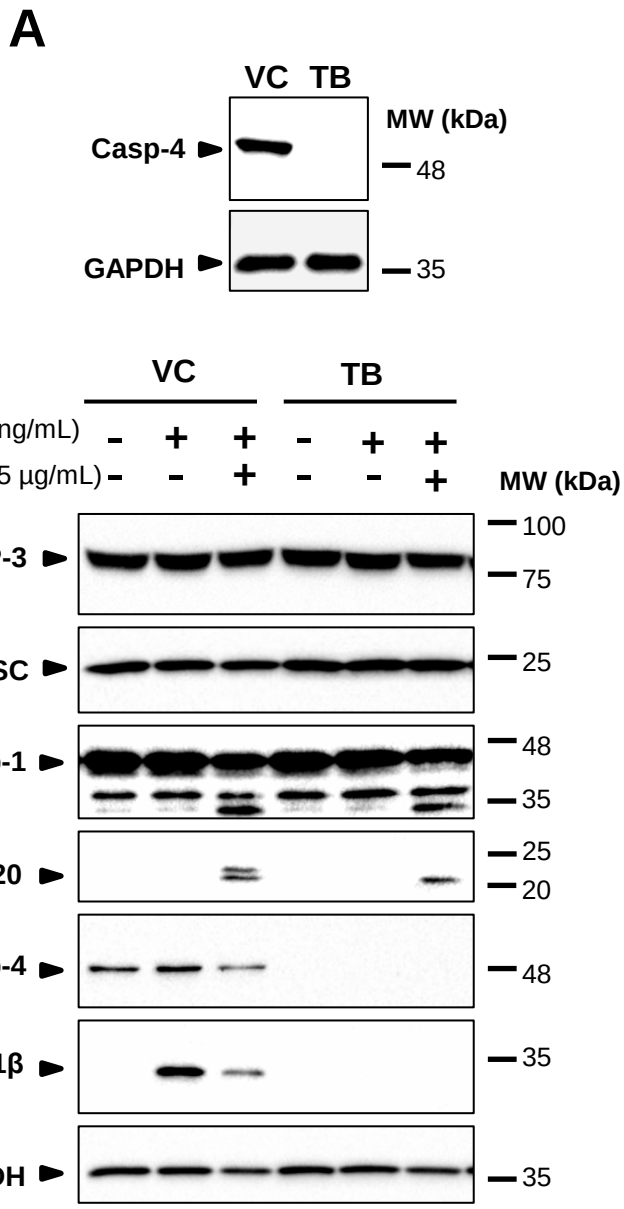

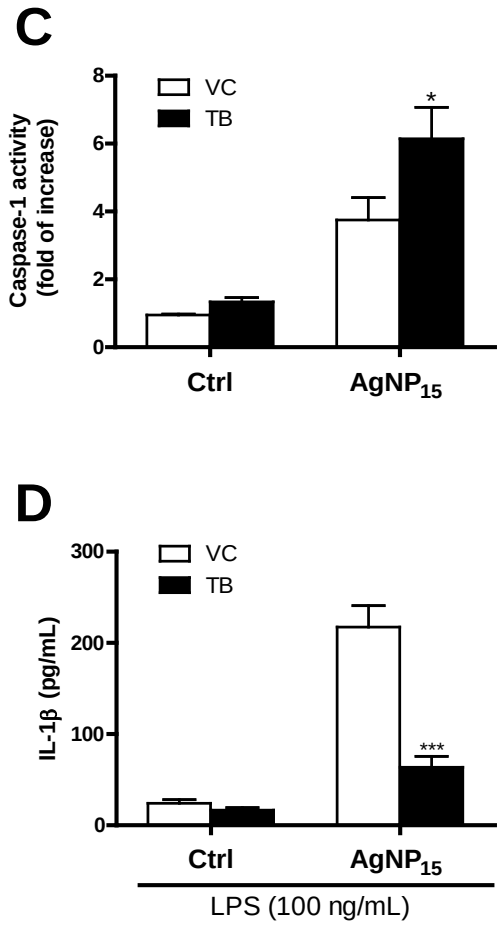

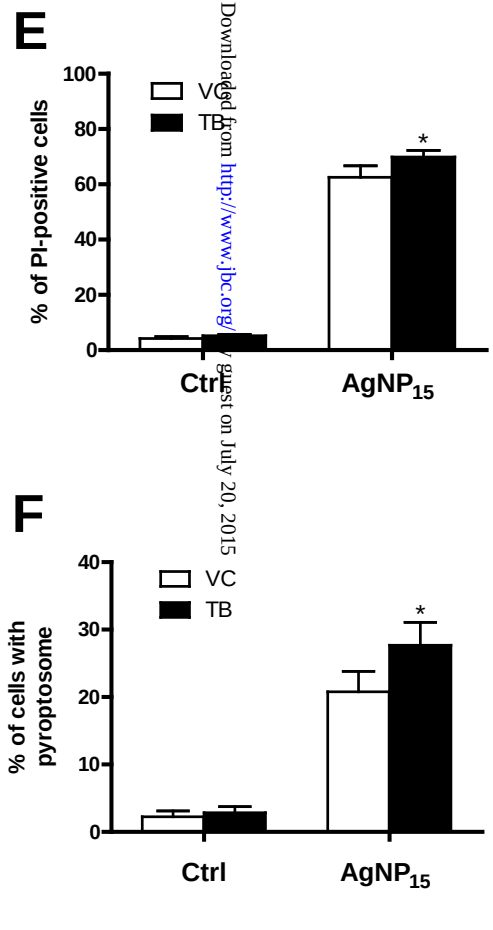

Figure 10

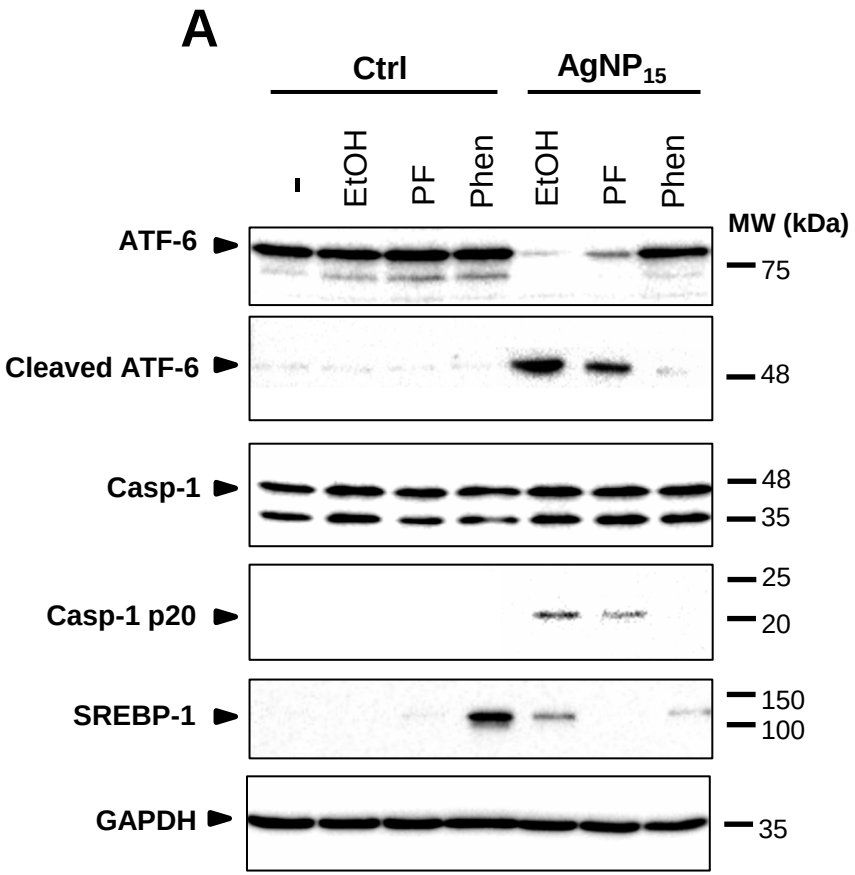

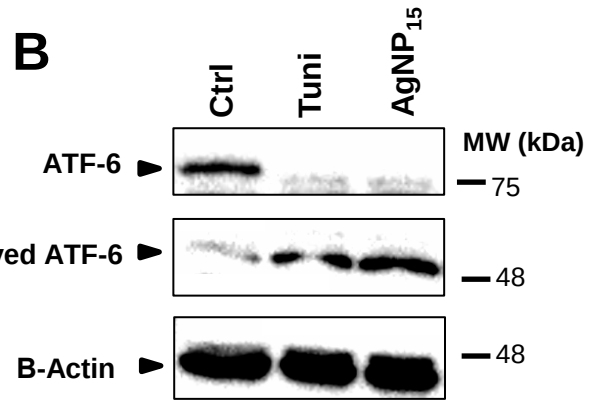

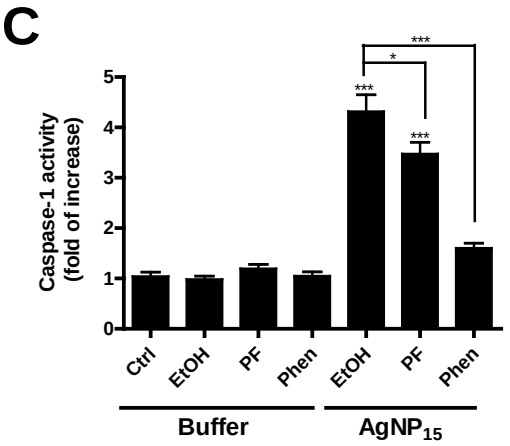

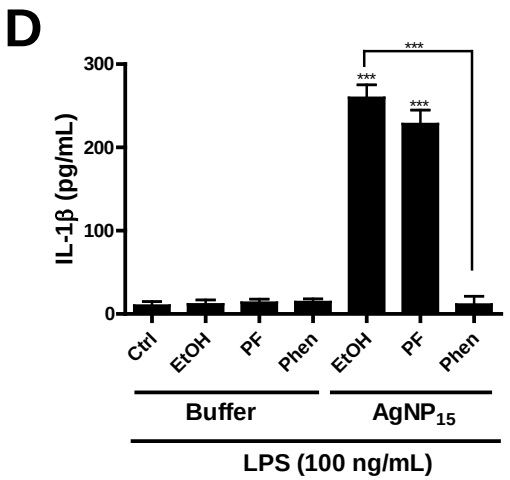

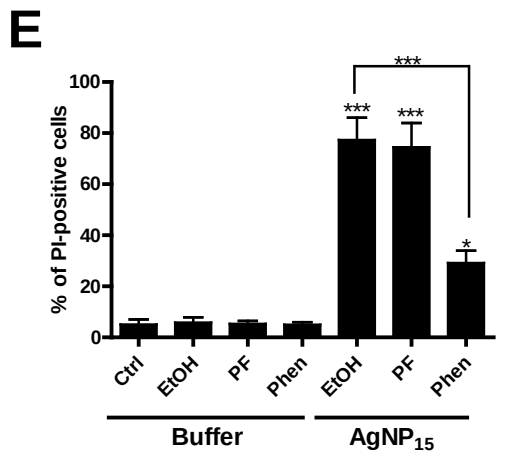

Figure 11

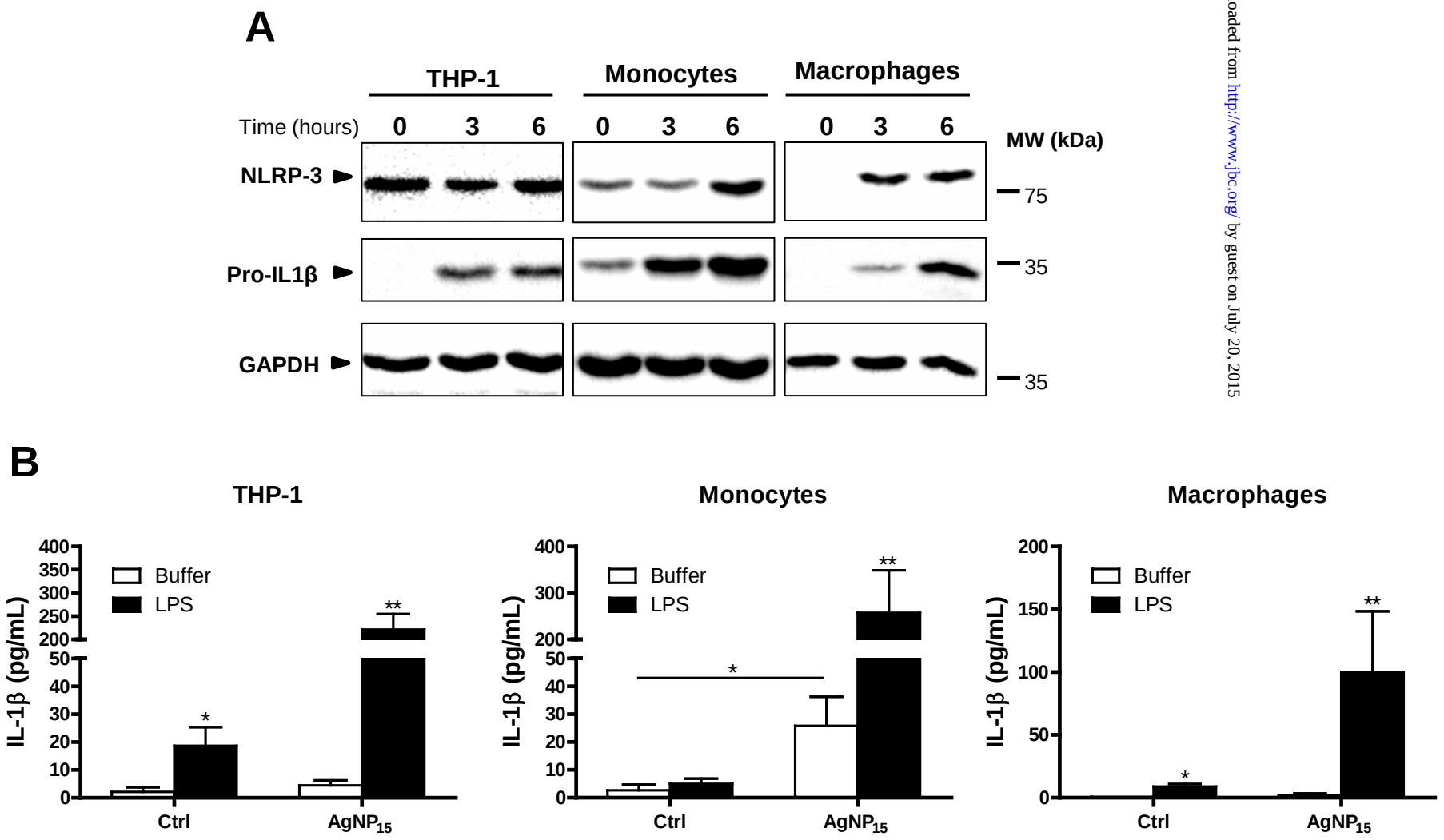

Cell Biology:

Silver Nanoparticles Induce Degradation of the Endoplasmic Reticulum Stress Sensor Activating Transcription Factor-6 Leading to Activation of the NLRP-3 Inflammasome

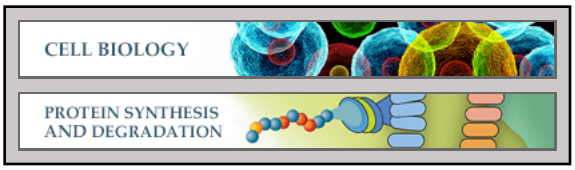

Jean-Christophe Simard, Francis Vallieres, Rafael de Liz, Valerie Lavastre and Denis Girard

J. Biol. Chem. *published online January 15, 2015*

Access the most updated version of this article at doi: 10.1074/jbc.M114.610899